

EXPERIMENTAL STUDY OF ACID FRACTURE CONDUCTIVITY OF AUSTIN
CHALK FORMATION

A Thesis

by

ANDREA NINO PENALOZA

Submitted to the Office of Graduate Studies of
Texas A&M University
in partial fulfillment of the requirements for the degree of

MASTER OF SCIENCE

Approved by:

Chair of Committee,	Ding Zhu
Co-Chair of Committee,	Dan Hill
Committee Member,	Victor Ugaz
Head of Department,	Dan Hill

May 2013

Major Subject: Petroleum Engineering

Copyright 2013 Andrea Nino Penaloza

ABSTRACT

Acid fracture conductivity and the effect of key variables in the etching process during acid fracturing can be assessed at the laboratory scale. This is accomplished by using an experimental apparatus that simulates acid injection fluxes comparable to those in actual acid fracture treatments. After acid etching, fracture conductivity is measured at different closure stresses.

This research work presents a systematic study to investigate the effect of temperature, rock-acid contact time and initial condition of the fracture surfaces on acid fracture conductivity in the Austin Chalk formation. While temperature and rock-acid contact are variables normally studied in fracture conductivity tests, the effect of the initial condition of the fracture surface has not been extensively investigated.

The experimental results showed that there is no significant difference in acid fracture conductivity at high closure stress using smooth or rough fracture surfaces. In addition, we analyzed the mechanisms of acid etching and resulting conductivity creation in the two types of fracture surfaces studied by using surface profiles. For smooth surfaces, the mechanism of conductivity creation seems connected to uneven etching of the rock and roughness generation. For rough surfaces, acid conductivity is related to smoothing and deepening of the initial features on the sample surface than by creating more roughness. Finally, we compared the experimental results with Nirode-Kruk correlation for acid fracture conductivity.

DEDICATION

To my family for their unconditional support during my graduate studies, especially to my mom who always believed in the true value of education and encouraged me to reach my goals.

ACKNOWLEDGEMENTS

I would like to express my gratitude to my advisors Dr. Ding Zhu and Dr. Dan Hill for their continuous guidance and support throughout the course of this research.

Thanks to Dr. Victor Ugaz for his time serving on my committee and to Dr. Maria Barrufet for serving as substitute member during my thesis defense. Thanks also go to my friends and colleagues who work on experimental research for their advices and help. My sincere appreciations to John Maldonado, the facilities team, and IT group at the Department of Petroleum Engineering for their technical support while doing this research work. I also want to extend my gratitude to the Crisman Institute at the Department of Petroleum Engineering for funding this study and Baker Hughes Incorporated for providing economical support during my graduate studies through the “Paula Erazo-Gonzalez” fellowship.

Finally, thanks to my family and to my boyfriend Andrew for their encouragement and love.

NOMENCLATURE

A_f	fracture Area, L^2 , in ² [m ²]
De	effective diffusion coefficient, L^2/t , cm ² /s
De^∞	effective diffusion coefficient, L^2/t , cm ² /s
d	diameter of the projected are of indentation, L, in
h_f	fracture height, L, in
k_f	fracture permeability, L^2 , md [m ²]
k_{fw}	fracture conductivity, L^3 , md-ft
$(k_{fw})_m$	matrix conductivity, L^3 , md-ft
k_m	matrix permeability, L^2 , md
l_f	fracture length, L, in [m]
pH	potential of Hydrogen
q_w	water flow rate, L^3/t , L/min [m ³ /s]
V_1	volume of rock removed after tensile fracture creation, L^3 , in ³
V_2	volume of rock removed after tensile fracture creation and acid injection, L^3 , in ³
V_{etched}	volume of rock etched by the acid, L^3 , in ³
W	load, mL/t ² , KN
w_f	fracture width, L, in
w_i	ideal fracture width, L, cm

Abbreviations

DREC	dissolved rock equivalent conductivity, L^3 , md-in
RES	rock embedment strength, m/Lt^2 , psi
TVD	true vertical distance, L, ft
UCS	unconfined compressive stress, m/Lt^2 , psi
wt	weight by weight ratio, m/m

Greek

μ_w	water viscosity, m/Lt , cP [Pa.s]
ΔP	pressure drop, m/Lt^2 , psi [Pa]
ΔP_{avg}	average pressure, m/Lt^2 , psi
ΔP_{min}	minimum pressure drop, m/Lt^2 , psi
ΔP_{max}	maximum pressure drop, m/Lt^2 , psi
σ_c	closure stress, m/Lt^2 , psi

TABLE OF CONTENTS

	Page
ABSTRACT	ii
DEDICATION.....	iii
ACKNOWLEDGEMENTS	iv
NOMENCLATURE	v
TABLE OF CONTENTS	vii
LIST OF FIGURES	ix
LIST OF TABLES.....	xii
CHAPTER I INTRODUCTION	1
1.1 Introduction.....	1
1.2 Literature Review	2
1.2.1 Acid Fracture Conductivity	2
1.2.2 Effect of Treatment Variables on Acid Fracture Conductivity	5
1.2.3 Linear Gelled Acid	5
1.2.4 Austin Chalk Formation.....	7
1.3 Problem Description.....	8
1.4 Objectives of Research.....	9
CHAPTER II EXPERIMENTAL SET UP, PROCEDURE, AND CONDITIONS.....	10
2.1 Experimental Set Up	10
2.1.1 Acid Injection Equipment	10
2.1.2 Profilometer.....	12
2.1.3 Point Load Test Apparatus.....	14
2.1.4 Fracture Conductivity Equipment	15
2.2 Experimental Procedure	16
2.2.1 Core Sample Preparation	17
2.2.2 Cores Scanning	23
2.2.3 Rock Embedment Strength Measurement	24
2.2.4 Acid Injection	26
2.2.5 Acid Fracture Conductivity Measurements.	30
2.3 Experimental Design	34

CHAPTER III RESULTS AND DISCUSSION	36
3.1 Basic Petrophysical Characterization of the Austin Chalk Cores.....	36
3.2 Experimental Results and Discussion	37
3.2.1 Low Temperature Level.....	38
3.2.2 High Temperature Level.....	43
3.2.3 Experimental Results vs. Nirode & Kruk Correlation.....	47
CHAPTER IV CONCLUSIONS AND RECOMMENDATIONS.....	51
4.1 Conclusions.....	51
4.2 Recommendations	52
REFERENCES	53
APPENDIX A	56
APPENDIX B.....	74
APPENDIX C.....	77

LIST OF FIGURES

	Page
Fig. 1—Austin Chalk trend and main producer fields (Martin et al. 2011).....	7
Fig. 2—Detailed schematic of acid injection in the modified API conductivity cell.....	11
Fig. 3—Schematic of acid injection set up (After Melendez 2007b).	12
Fig. 4—Profilometer.	13
Fig. 5—Photograph and scanned surface of cores after acid injection.....	13
Fig. 6—PL-100 for Rock Embedment Strength measurements.....	14
Fig. 7—Detailed schematic of acid fracture conductivity measurements.	15
Fig. 8—Schematic of acid fracture conductivity set up.....	16
Fig. 9—Experimental procedure for acid fracture conductivity measurements (After Melendez 2007b).....	17
Fig. 10—Core dimensions.....	18
Fig. 11—Preparation of composite cores. (a) Austin Chalk and high permeability cores, (b) Application of glue on internal surfaces, (c) Composite cores.	19
Fig. 12—Application of weight on composite cores.	19
Fig. 13—Tape protecting fracture and bottom surface from silicon.	20
Fig. 14—Application of silicon premier on core walls.....	21
Fig. 15—Silicon release agent being applied to molds.....	21
Fig. 16—Pouring silicon inside the molds.	22
Fig. 17—Scanned fracture surfaces of rough surface core. (a) Before acid injection, (b) After acid injection.....	24

Fig. 18—Etched fracture surfaces of smooth surface cores. (a) 5 minutes of rock-acid contact at 100 °F, (b) 10 minutes of rock-acid contact at 100 °F.	38
Fig. 19—Fracture surfaces of rough surface core. (a) Before acid injection, (b) After 5 minutes of rock-acid contact at 100 °F.	39
Fig. 20—Fracture surfaces of rough surface core. (a) Before acid injection, (b) After 10 minutes of rock-acid contact at 100 °F.	40
Fig. 21—Acid fracture conductivity for experiments at 100 °F.....	41
Fig. 22—Etched fracture surfaces of smooth surface cores. (a) 5 minutes of rock-acid contact at 130 °F, (b) 10 minutes of rock-acid contact at 130 °F.	43
Fig. 23—Fracture surfaces of rough surface core. (a) Before acid injection, (b) After 5 minutes of rock-acid contact at 130 °F.	44
Fig. 24—Fracture surfaces of rough surface core. (a) Before acid injection, (b) After 10 minutes of rock-acid contact at 130 °F.	45
Fig. 25—Acid fracture conductivity for experiments at 130 °F.....	46
Fig. A-1—Profilometer controls input screen (before run button is clicked).....	56
Fig. A-2—Profilometer controls input screen (after run button is clicked).....	57
Fig. A-3—Surface plot for experiment RS2B.....	60
Fig. A-4—Front panel of Acid Frac Injection.vi.....	61
Fig. A-5—Front panel of Acid Frac Conductivity.vi.	62
Fig. A-6—Selecting Show Block Diagram panel.....	62
Fig. A-7—Opening object to save .lvm file.	63
Fig. A-8—Saving .lvm files.	63
Fig. A-9—Detection DAC.	65
Fig. A-10—Selection of device to be calibrated.	66
Fig. A-11—Testing device for 0 psi. Initial point.	67

Fig. A-12—Linear regression to calculate slope and intercept for calibration line.	68
Fig. A-13—Scale selection panel.	68
Fig. A-14—Calibration data for preexisting scale.....	69
Fig. A-15—Wizard for creation of new calibration scale.....	70
Fig. A-16—Calibration data for new scale.	71
Fig. A-17—Voltage selection.....	72
Fig. A-18—Scale selection.....	72
Fig. B-1—Schematic for permeability measurements using conductivity cell.....	75
Fig. C-1—Top etched fracture surfaces and V_{etched} values of smooth surface cores. (a) 5 minutes of rock-acid contact at 100 °F, (b) 10 minutes of rock-acid contact at 100 °F.....	77
Fig. C-2—Top etched fracture surfaces and V_{etched} values of rough surface cores. (a) After 5 minutes of rock-acid contact at 100 °F, (b). After 10 minutes of rock-acid contact at 100 °F.....	77
Fig. C-3—Top etched fracture surfaces and V_{etched} values of smooth surface cores. (a) 5 minutes of rock-acid contact at 130 °F, (b) 10 minutes of rock-acid contact at 130 °F.....	78
Fig. C-4—Top etched fracture surfaces and V_{etched} values of rough surface cores. (a) After 5 minutes of rock-acid contact at 130 °F, (b). After 10 minutes of rock-acid contact at 130 °F.....	78

LIST OF TABLES

	Page
Table 1—Experimental design.	34
Table 2—Parameter values used in Ramey’s equations.	35
Table 3—Basic petrophysical characterization of the Austin Chalk cores.	37
Table 4—Young modulus and Poisson ratio of Austin Chalk cores.	37
Table 5—Summary of V_{etched} values for experiments at 100 °F.	40
Table 6—Summary rock embedment strength values for experiments at 100 °F.	42
Table 7—Summary of V_{etched} values for experiments at 130 °F.	45
Table 8—Summary rock embedment strength values for experiments at 130 °F.	47
Table 9—Acid fracture conductivity results at 100 °F compared to Nirode and Kruk correlation.	49
Table 10—Acid fracture conductivity results at 130 °F compared to Nirode and Kruk correlation.	50
Table B-1—Values of variables used in matrix conductivity calculation.	76

CHAPTER I

INTRODUCTION

1.1 Introduction

Acid fracturing is a stimulation technique used to increase production rates and improve ultimate recovery in carbonate reservoirs. This technique involves hydraulically fracturing the formation and then injecting an acid fluid which dissolves the carbonate minerals present in the formation. The chemical reaction leads to a creation of differential etching along the fracture surfaces which contributes to increase the flow capacity of the fracture.

Acid fracture conductivity is a measure of the flow capacity through an acidized fracture. The fracture conductivity is affected by the amount of rock dissolved by the acid, the non-uniform etching on the fracture surfaces, and the strength of the rock. The main objective of acid fracturing is to make the acidized fracture a permanent conductive flow path that endures the overburden pressure and effectively connects the reservoir to the wellbore.

The goal of this study is to investigate the influence of key variables on the etching process and on the resulting acid fracture conductivity at the laboratory scale. The experimental procedure is divided in stages. It starts with the injection of an acid fluid along an artificial fracture with a controlled leak-off rate. The injection fluxes used in the laboratory are comparable to those in actual acid fracturing treatments. The next stage is the characterization of the acid etching on the fracture surfaces, achieved with a

profilometer. Finally, fracture conductivity is measured at incremental closure stresses until matrix conductivity is reached.

We conducted a systematic study using core samples from an outcrop of the Austin Chalk formation to investigate the effect of temperature, rock-acid contact time, and the initial condition of the fracture surfaces on acid fracture conductivity. While temperature and rock-acid contact are variables normally studied in fracture conductivity tests, the effect of the initial condition of the fracture surface has not been extensively investigated in the past.

1.2 Literature Review

1.2.1 Acid Fracture Conductivity

Acid fracture conductivity is difficult to predict because it inherently depends on a stochastic process and is affected by several parameters. Therefore, a common approach is to follow an experimental methodology to measure and study acid fracture conductivity. Broaddus et al. (1968) conducted the first laboratory work on acid fracture conductivity. They concluded that acid fracture conductivity is a function of the acid type, acid concentration, acid-rock contact time, formation type, and temperature.

Since this study was conducted, the aforementioned factors have been frequently documented throughout the literature. Previous experimental studies suggested that acid fracture conductivity is related to these factors through the etched pattern created by the acid on the fracture faces and the strength of the rock retained after acid injection (Beg,

et al. 1998; Pournik et al. 2007; Melendez et al. 2007a; Pournik et al. 2010; Gomaa and Nasr-El-Din 2009).

The etched pattern is an important outcome from experimental work on acid fracture conductivity. The initial condition of the fracture surfaces can be smooth or rough. Smooth surfaces are created with a wet saw while rough surfaces are generated by fracturing a core with a chisel. Experimental work has been carried out using both types of surfaces, but mostly on smooth surfaces. As reported by Smith et al. (1970), the aim of using smooth surfaces is to investigate conductivity in heterogeneous formations. For this case, the etched pattern will be the result of an uneven reaction that will dissolve some areas in greater extent than others due to differences in the mineralogical composition of the rock.

Later in 1973, Nierode and Kruk conducted experiments using core plugs that have 1 inch in diameter and 2 to 3 inches long, with rough fracture surfaces and no fluid loss. After the injection of acid emulsions and viscous acids, they found that conductivity occurred primarily because of the smoothing of some peaks of the rock surfaces and the mismatch of the fracture features after applying closure stress. Only limited effects were found as a result of rock heterogeneities, apparently caused by the small sample size used in the test.

Nierode and Kruk (1973) also developed a correlation for acid fracture conductivity that is widely used for its simplicity but it is not accurate all the times. This correlation is shown in Eqs. 1, 2, and 3.

$$k_f w = C_1 \exp(-C_2 \sigma_c) \dots \dots \dots (1)$$

$$C_1 = 0.265 (DREC)^{0.822} \dots\dots\dots(2)$$

$$C_2 \times 10^3 = \begin{cases} 19.9 - 1.3\text{Ln}(\text{RES}) & 0 < \text{RES} < 20,000 \text{ psi} \\ 3.8 - 0.28\text{Ln}(\text{RES}) & 20,000 \leq \text{RES} \leq 500,000 \text{ psi} \end{cases} \dots\dots\dots(3)$$

Where k_{fw} is the fracture conductivity in md-in, σ_c is the fracture closure stress in psi, DREC is the dissolved rock equivalent conductivity in md-in, and RES is the rock embedment strength in psi. RES is defined as the force required to indent a steel ball into a rock surface to a distance equal to the half radius of the ball, divided by its projected area (Howard and Fast 1970). DREC can be calculated with Eq. 4 (Melendez 2007b):

$$DREC = \frac{w_i^3 \times 10^{11}}{30} \dots\dots\dots(4)$$

The ideal fracture width w_i in cm., is obtained by dividing the volume of rock etched by the acid (V_{etched}) by the fracture area (A_f).

The resulting plot of Eq. 1 is a straight line where C_1 is the intercept with y-axis and C_2 is the slope. C_1 depends on DREC while C_2 depends on RES. The correlation predicts that as DREC increases, the value of C_1 increases, which leads to higher initial conductivities. This is not entirely true as suggested by Beg et al. (1998) who found that long rock-acid contact times do not always increase fracture conductivity. On the other hand, Eqs. 1 and 3 suggests that high values of RES yield low values of C_2 which represents slower decline on conductivity with closure stress. However, there are no studies published about the effect that smooth and rough fracture surfaces have on the reduction of conductivity and the role that RES plays in these cases.

1.2.2 Effect of Treatment Variables on Acid Fracture Conductivity

The effect of temperature and rock-acid contact time on acid fracture conductivity has been extensively studied in different formations types. Melendez (2007b) conducted experimental work in limestone, chalk, and dolomitic formations. She observed that large rock-acid contact times and high treatment temperatures did not necessarily correlate with high fracture conductivity values. These observations point out the importance of considering formation cooling effects instead of using reservoir temperatures when conducting the experiments. Also, these laboratory observations indicate the necessity of reducing the rock-acid contact times to match current acid pumping schedules in the field.

Regarding the initial condition of the fracture surface, Nierode et al. (1972) reported that the acid diffusion coefficients for rough surfaces are larger than for smooth surfaces. However, they did not document the effect that these results would have in acid fracture conductivity values. Recently, Neumann (2011) reported that when smooth fracture surfaces develop channel-type etched pattern, they retain higher conductivity than rough fracture surfaces at high closure stress. Considering these outcomes, a systematic study is needed to develop a greater understanding of the effect that the initial condition of the fracture surface has on acid fracture conductivity.

1.2.3 Linear Gelled Acid

Hydrochloric acid at 15 and 28 %wt. is commonly used for acid fracturing in carbonate reservoirs. The reaction products are water soluble and easily removed from

the formation. The heterogeneous reaction involving hydrochloric acid and calcite follows Eq. 5 (Lund et al. 1974):



Hydrochloric acid is highly reactive with calcite, the main component in the Austin Chalk formation. The high reaction rate limits the acid penetration distance in the fracture because most of the acid leaks into the permeable formation. In order to decrease the leak-off into the formation and retard the reaction rate, polymers are used to increase the viscosity of hydrochloric solutions.

Suitable polymers for acid fracturing should contain carboxyl groups. Also, they must exhibit stability in aqueous acid solutions and at the treating temperature (Crowe 1987). Copolymers of acrylamide fulfill the previously noted conditions and they were used to prepare the linear gelled acid used in this research work. Gelled acids are mostly known by their retardation effect on the reaction rate between the acid and the fracture walls. In addition, gelled acids create a filter cake that can reduce the leak-off rate.

Linear gelled acids are prepared by adding a polymer, generally hydrated copolymers of acrylamide, to an acid solution. This acid solution is composed of water, corrosion inhibitor, iron control agent, and hydrochloric acid. The gelled acid will gain viscosity by the hydration of the polymer. This process is not instantaneous but usually takes approximately 30 minutes to reach the final viscosity after the polymer is added.

1.2.4 Austin Chalk Formation

The Austin Chalk formation extends throughout Texas, Louisiana, and Mississippi, parallel to the Gulf Coast (**Fig. 1**). It is a low-permeability fractured reservoir consisting of interbedded chinks, volcanic ash, and marls (Martin et al. 2011). The Austin Chalk cores used in this study were collected from an outcrop located in the outskirts of Austin, Texas.



Fig. 1—Austin Chalk trend and main producer fields (Martin et al. 2011)

Chinks tend to be uniform and soft which cause difficulties in stimulation by acid fracturing. The differential etching after acid injection is generally low. Even when there is uneven etching, the formation closure stress can crush newly formed channels (Anderson and Fredrickson 1989). It is widely known that formations etched differently depending on the type of acid used. This has been the approach used in Austin Chalk

where gelled acids are pumped preferentially to reduce the acid reaction rate and increase acid penetration. A basic petrophysic characterization of outcrop used in this thesis work is presented in the Results and Discussion Chapter.

1.3 Problem Description

Experimental work to measure and study acid fracture conductivity can provide significant insights about the mechanisms of generation of conductivity in different formation types. Zhou (2006) and Melendez (2007b) modified the API conductivity cell in order to use bigger core samples to capture the effect that formation heterogeneities have on the etched pattern in smooth surface cores. However, recent publications questioned the validity of this experimental approach.

Neumann et al. (2012) studied the etched patterns created by straight HCl in carbonates from Brazilian cores and outcrops. They used smooth and rough fracture surfaces. On smooth surfaces, they observed the creation of uniform, rough, and channel-type etched patterns. These patterns were previously identified and classified by Pournink et al. (2007) and Antelo et al. (2009). For the rough surfaces, Neumann et al. (2012) detected the smoothing of peaks instead of the creation of roughness by the acid reaction. Based on these observations, they concluded that acid conductivity is not related to asperities or roughness generation. Moreover, they suggested that the creation of patterns is an artifact of using smooth fracture surfaces.

Certainly, using rough fracture surfaces more accurately represent the fracture walls after hydraulic fracturing. However, it is important to conduct a systematic study

to understand the differences, if any, of acid fracture conductivity when using smooth and rough fracture surfaces at the same experimental conditions. This can provide a better understanding of the mechanisms of conductivity creation and their impact on the reduction of conductivity with closure stress for both types of surfaces.

Finally, the systematic study must also investigate the effect of temperature and rock-acid contact time on the resulting acid fracture conductivity for each of the type of fracture surfaces investigated.

1.4 Objectives of Research

Fracture conductivity experiments were performed using an experimental facility that properly scale acid injection and leak-off fluxes to those compared in actual acid fracturing treatments. Austin Chalk cores were used as well as a linear gelled acid of extended used in this prolific formation. Two main objectives were identified for the present research work:

- Conduct a systematic study to investigate the effect of temperature and rock-acid contact time on fracture conductivity in Austin Chalk. Formation cooling effects and contact times that match current pumping schedules were considered in the creation the experimental matrix.
- Determine if there is a substantial difference between the values of conductivity measured for smooth and rough fracture surfaces at the same experimental conditions. The mechanisms of conductivity creation will be characterized for both surface types. .

CHAPTER II

EXPERIMENTAL SET UP, PROCEDURE, AND CONDITIONS

This chapter describes the equipment and experimental procedure used to study acid fracture conductivity in the Austin Chalk formation. The experimental conditions determined for this study are presented and discussed at the end of the chapter.

2.1 Experimental Set Up

The experimental set up used in this research work is comprised of an acid injection facility, a profilometer, a point load test apparatus, and a fracture conductivity measurement equipment. A description of each component within the experimental set up is presented below.

2.1.1 Acid Injection Equipment

The center of the acid injection equipment is the modified API conductivity cell which accommodates larger cores than specified in the API RP-61 (Zhou 2006). The new core dimensions are 7 in. long, 1.7 in. wide and 3 in. in thickness. The cell employed herein is made of Hastelloy C-276 material which is resistant to acid corrosion.

A pair of cores is placed inside the conductivity cell vertically to avoid gravitational effects on the diffusivity coefficients during the acid reaction. Live acid

flows through an artificial fracture of 0.12 in. wide and through the porous media of the core samples as shown in **Fig. 2**.

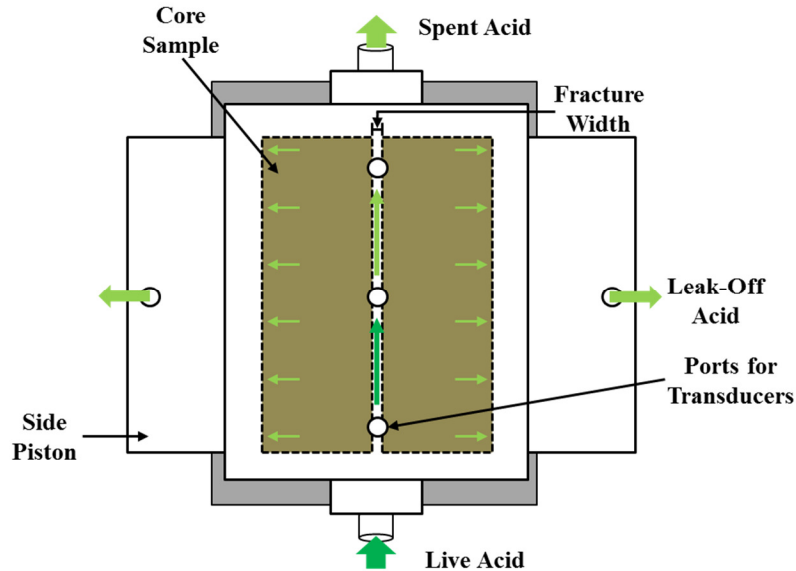


Fig. 2—Detailed schematic of acid injection in the modified API conductivity cell.

A schematic of the acid injection facility is shown in **Fig. 3**. A heating jacket is used to warm up the cell body while a heating tape is used to pre-heat the acid at the desired temperature. The cell pressure is kept constant at 1000 psi to maintain the CO₂ generated from the acid reaction in solution. The cell and the leak-off pressures are controlled with back pressure regulators. The volume of acid leaking through the cores is measured. Three pressure transducers display the pressure in the system during the acid injection and are connected to a data acquisition system. One pressure transducer monitors the pressure in the cell; the other two transducers monitor the pressure drop across the fracture and leak-off. A diaphragm pump delivers a maximum injection rate of 1 liter per minute, which is equivalent to 20 barrels per minute in the field (Pournik

2008). The pump is connected to a water tank and an acid tank. Prior to the acid injection, the systems is flushed and warmed-up with water. Once the system reaches the desired temperature and pressure, the valves are switched and acid is pumped to the cell.

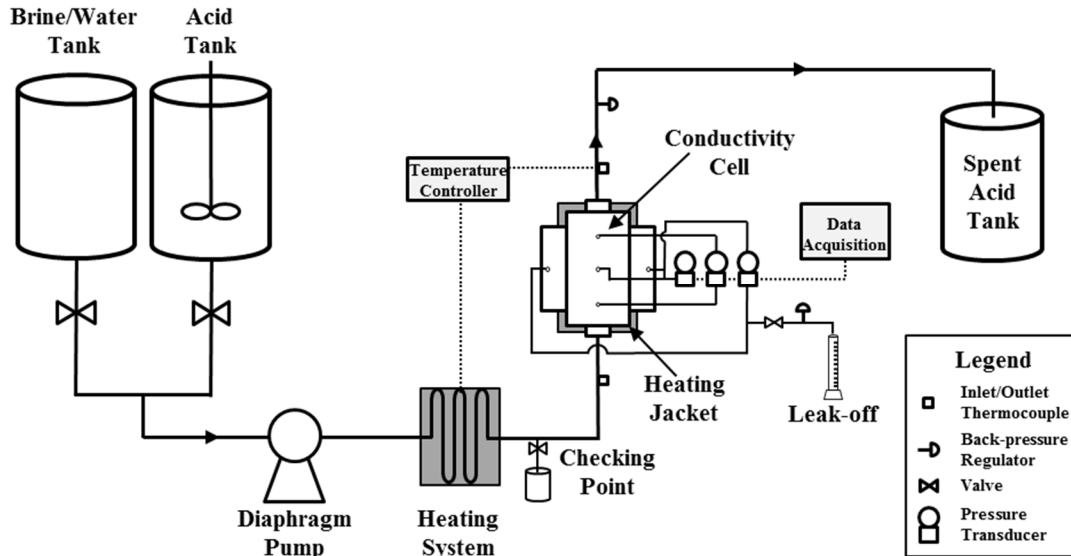


Fig. 3—Schematic of acid injection set up (After Melendez 2007b).

2.1.2 Profilometer

The profilometer is composed of a laser sensor, a servo-table, and a control box as shown in **Fig. 4**. The laser measures minute surface variations as a function of the position on the fracture surface. The resolution of the vertical measurement is 0.002 in; the horizontal X and Y resolution is 0.05 in.

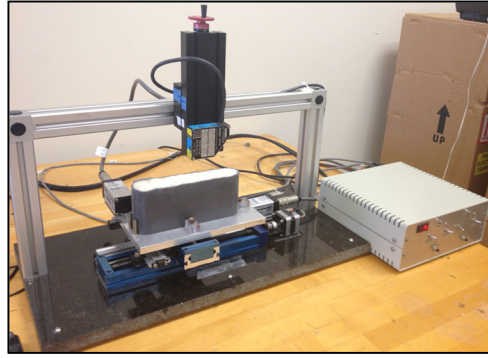


Fig. 4—Profilometer.

The data captured by the laser sensor is converted to a matrix to calculate the volume of rock dissolved by the acid (V_{etched}). Moreover, this data is used to create 3D images of the fracture surface as shown in **Fig. 5**. The V_{etched} and the 3D images are generated with a program developed in Matlab. More details about the functionality of the profilometer are explained in Malagon (2007). The operating procedure for the profilometer can be found in Appendix A.

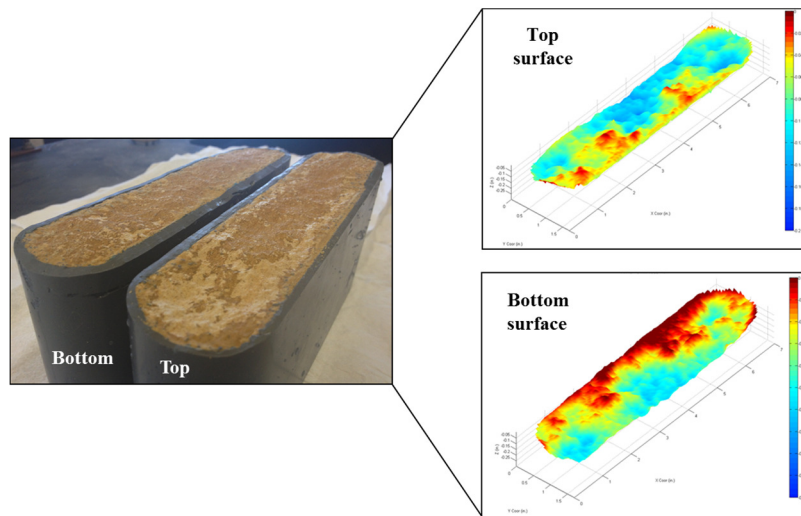


Fig. 5—Photograph and scanned surface of cores after acid injection.

2.1.3 Point Load Test Apparatus

A Point Load Test System PLT-100 was used to measure rock embedment strength before and after acid injection for some of the experiments. This test was performed following the experimental procedure mentioned in Howard and Fast (1970). The PLT-100 is shown in **Fig. 6** as well as the steel ball ready to be indented on the core plug surface.



Fig. 6—PL-100 for Rock Embedment Strength measurements.

The PLT-100 is constituted by a load frame, a set of two load platens, and a hydraulic jack to raise the bottom platen. It also has a control box with a digital display for the load applied to the core plugs.

2.1.4 Fracture Conductivity Equipment

For conductivity measurements, the cell is placed horizontally in a load frame which provides pressure in the perpendicular direction to the fracture. This pressure represents the closure stress in a fractured formation. The acidized fracture surfaces are placed in contact to each other and water is pumped at a constant flow rate through the remaining fracture width as shown in **Fig. 7**.

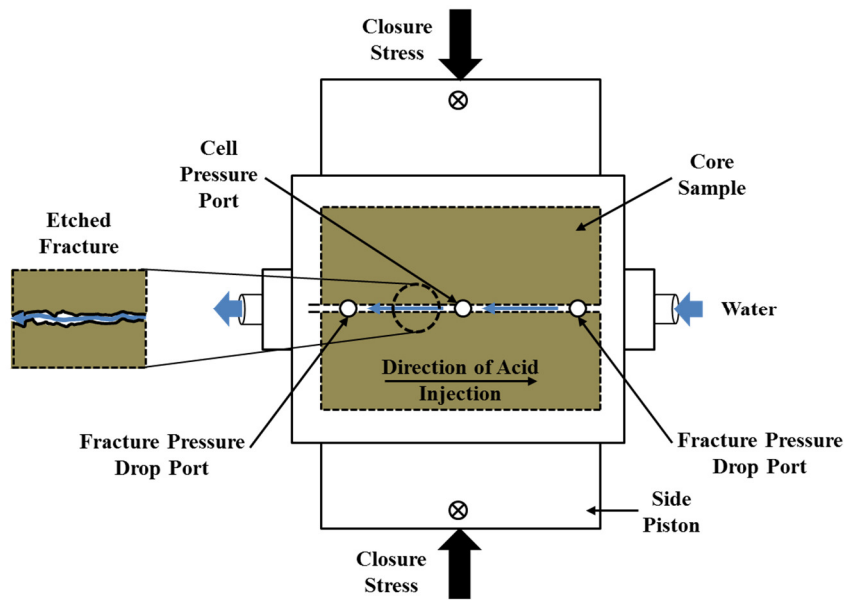


Fig. 7—Detailed schematic of acid fracture conductivity measurements.

A schematic of the fracture conductivity equipment is shown in **Fig. 8**. This set-up has pressure transducers for different pressure drop ranges; 0-10 psi, 0-30 psi, and 0-150 psi. For a given closure stress, two pressure transducers are used. One pressure transducer measures the cell pressure in a port located in the center of the cell as shown in Fig. 8. The second transducer measures the pressure drop across the fracture

illustrated in Fig. 8. Once the pressure drop reaches a constant value, the conductivity of the acidized fracture is calculated using Darcy's flow equation.

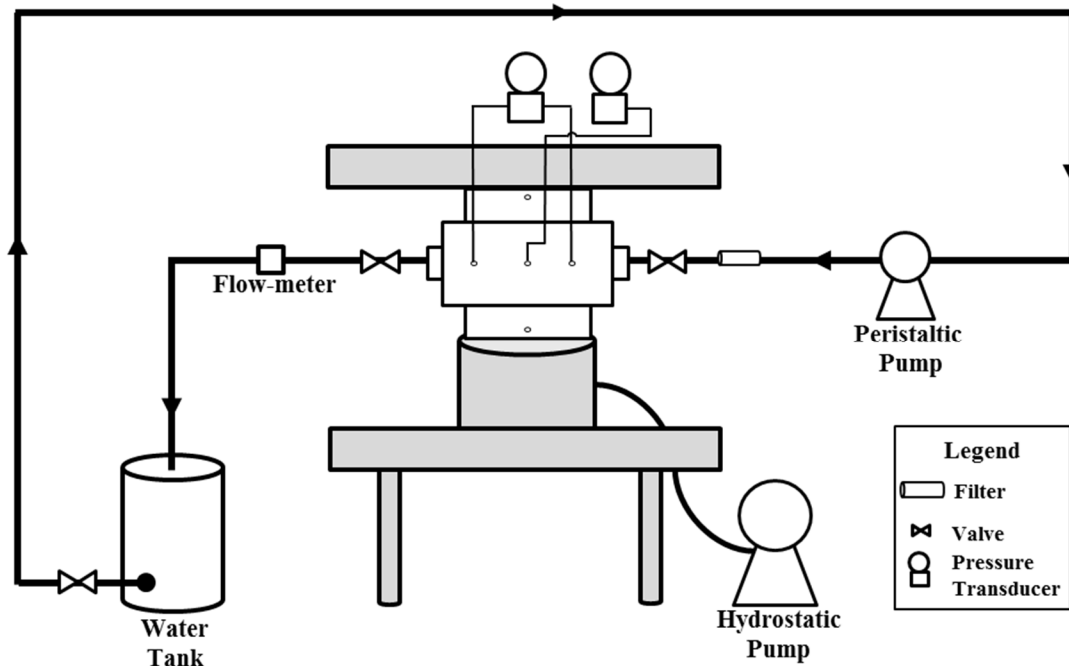


Fig. 8—Schematic of acid fracture conductivity set up.

2.2 Experimental Procedure

Measuring the variation in acid fracture conductivity with closure stress is the final phase of each experiment. Seven steps are followed to achieve this goal as shown in **Fig. 9**. The description of each step is explained in the next sections.

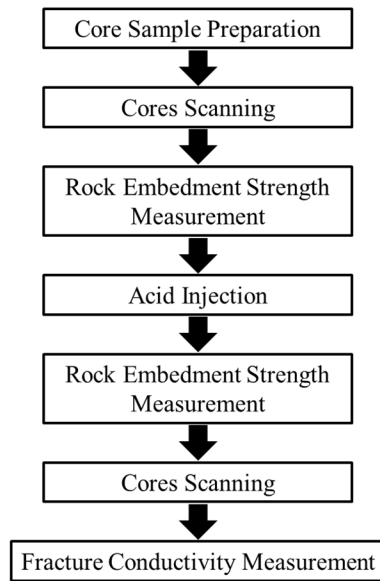


Fig. 9—Experimental procedure for acid fracture conductivity measurements (After Melendez 2007b).

2.2.1 Core Sample Preparation

The experimental procedure starts with the preparation of the cores samples. The purpose is to coat the rock samples with a silicon mix that isolates the walls of the rock leaving only the top (fracture surface) and bottom sides exposed. The top side will be in direct contact with the acid while the acid leak-off will exit from the bottom side. Also, the coating offers a seal between the conductivity cell and the rock sample to avoid leaks during the acid injection and conductivity measurements.

The procedure for preparing core samples is explained in detail by Melendez (2007b). However, some modifications were done to this procedure in order to improve the adherence between the silicon and rock, and to address the sample preparation of

composite cores in the case of rough fracture surface cores. For an experiment a pair of core samples with 7 in. long, 1.7 in. wide, and 3 in. in thick are used (**Fig. 10**).

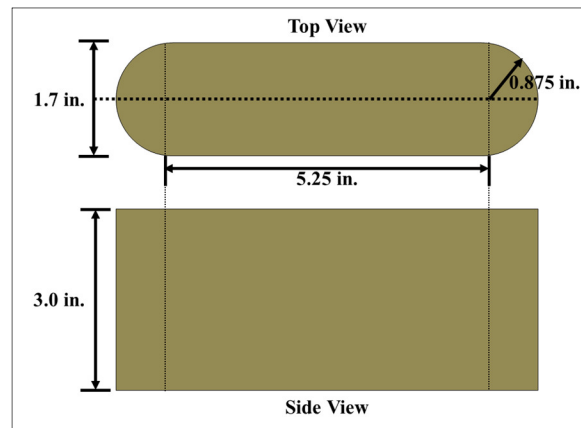


Fig. 10—Core dimensions.

A detailed procedure for the core samples preparation is enumerated below:

- Clean the core surface with a brush to remove dust produced during the cutting process.
- Build a composite core if there is not enough rock to create a 3-in. thick core sample as shown in **Fig. 11**. Glue the top (study rock) and bottom core (high permeability rock) by their internal surfaces.

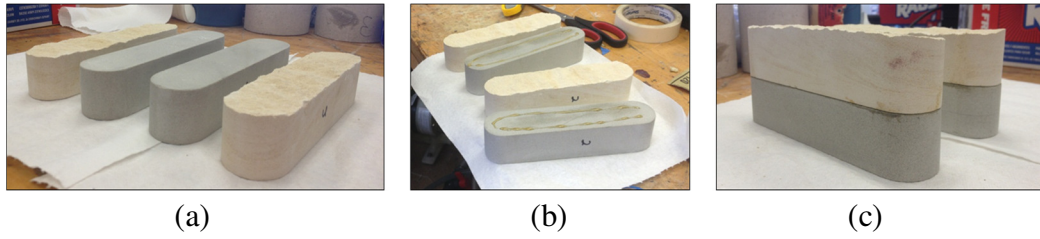


Fig. 11—Preparation of composite cores. (a) Austin Chalk and high permeability cores, (b) Application of glue on internal surfaces, (c) Composite cores.

- Apply some weight to the composite cores to avoid shifting of the rock surfaces unions by expansion of the glue (**Fig. 12**). Wait for 4 hours for the adhesive to dry.



Fig. 12—Application of weight on composite cores.

- Cover the top and bottom surfaces with paper tape (**Fig. 13**). Apply pressure on the fracture surface (top), especially if it is a rough fracture surface.

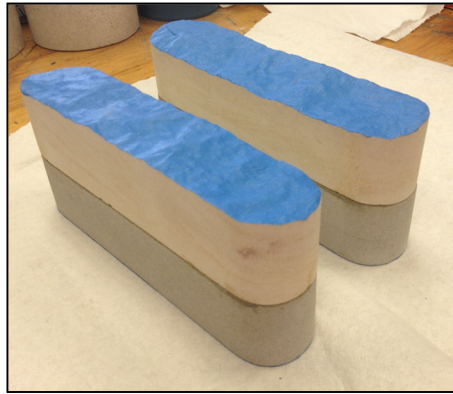


Fig. 13—Tape protecting fracture and bottom surface from silicon.

- Label the sample. For instance, use a number to identify the sample and also write down an arrow to indicate the direction in which the cores are going to be scanned which should be the same for acid injection.
- Mix in a ratio of 1:1 (weight or volume), of the silicone potting compound and the silicon curing agent. Let the blend sit for 20 minutes or until minimal bubbling is observed.
- Apply three layers of the silicone primer (SS4155) on the walls of the cores (**Fig. 14**). Wait 15 minutes between the application of each layer or until the primer is dried.

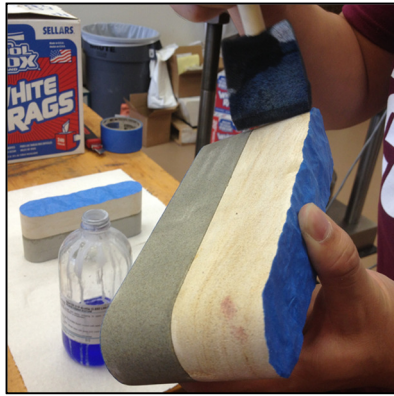


Fig. 14—Application of silicon premier on core walls.

- Clean the molds surfaces and plastic seals with acetone.
- Spray two layers of silicon releasing agent on the metal surface of the molds (**Fig. 15**). Wait 10 minutes between applying each layer.

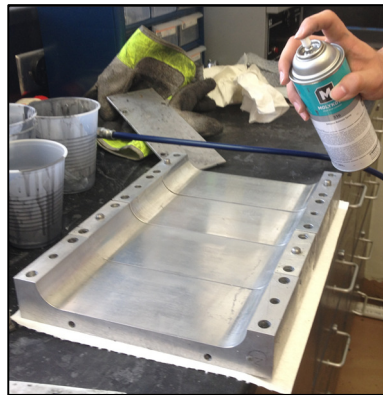


Fig. 15—Silicon release agent being applied to molds.

- Assemble the molds by attaching the bottom of the mold and the plastic seal with four bolts. Then, screw three more bolts in the sides of the mold.

- Pour a small amount of silicon onto the bottom of the mold.
- Place the core in the center of slot inside the mold and press the core against the bottom to displace the silicon applied in the previous step.
- Pour the silicon blend inside the gap between the mold and the core (**Fig. 16**).

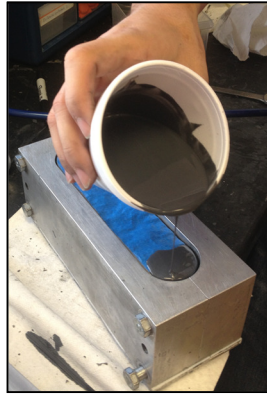


Fig. 16—Pouring silicon inside the molds.

- Let the silicon dry at ambient temperature. During this process, the silicon will adhere to the core surface before the curing process.
- Place the molds in the oven for two to three hours maximum at 212 °F (100 °C)
- Remove the molds from the oven. Let them cool down to ambient temperature.
- Remove the bolts and the plastic seal.
- Remove the cores from the mold.
- Remove the paper tape and silicon remaining in the top and bottom surface.
- Cut the silicon at the edges of the core surfaces carefully. Try to match the edges of the silicon to those of the core. When the silicon edges are over-cut, a path for water flow is created contributing to higher conductivity values.

2.2.2 Cores Scanning

Once the cores are coated, the top of the cores or accurately noted as the fracture surfaces are scanned with a profilometer. The scanning of the fracture surfaces is performed before and after the acid injection. For smooth surfaces, scanning before the acid injection establishes a base line that is compared to the fracture surface after being in contact with the acid. The data captured by the laser is converted to a matrix form. The matrix after acid injection is subtracted from the matrix before acid injection to yield the volume of rock dissolved by the acid (V_{etched}). A program developed in Matlab performs this calculation and delivers a 3D plot of the etched fracture surface.

In the case of rough fracture surfaces, subtracting the matrix after acid injection from the matrix before acid injection also yields the correct V_{etched} value. However, the 3D plots generated by Matlab are not correct. This is due to the base line or initial condition is no longer smooth. Therefore, an additional procedure in Matlab is necessary. First, the matrix of the rough surface before acid injection is subtracted from a reference smooth surface. This yields a volume difference that represents the rock removed when the tensile fracture was created, V_I . The 3D plot created from V_I features the initial condition of the tensile fracture surface before acid injection as shown in **Fig. 17a**.

Second, the matrix of the rough surface after acid injection is subtracted from the same smooth surface used in the step mentioned above. This volume difference represents the rock removed when the tensile fracture was created plus the rock dissolved by the acid created, V_2 . V_{etched} is calculated by subtracting V_I from V_2 . The 3D

plot created from V_2 features the final condition of the tensile fracture surface after acid injection as shown in **Fig. 17b**.

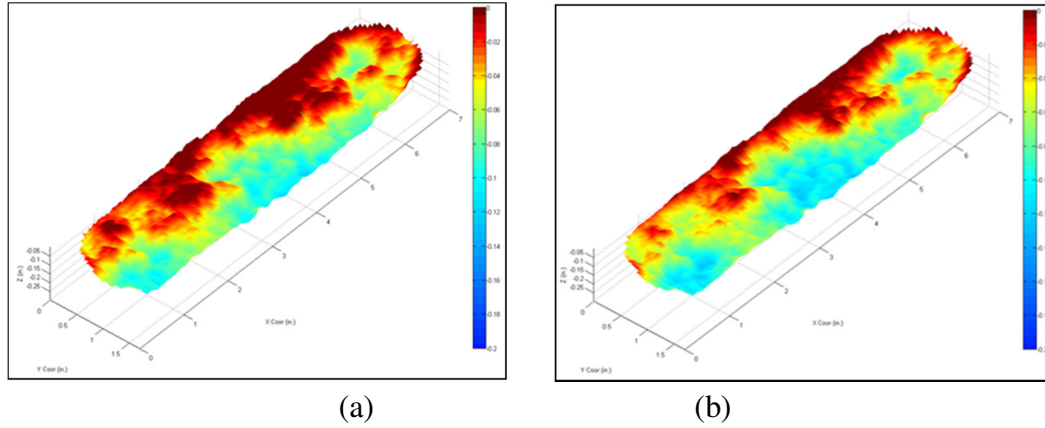


Fig. 17—Scanned fracture surfaces of rough surface core. (a) Before acid injection, (b) After acid injection.

2.2.3 Rock Embedment Strength Measurement

Melendez (2007b) presented a procedure to measure rock embedment strength (RES) at 28 points on each fracture surfaces. She found that the RES values fitted in a normal distribution curve and not significant difference of RES was observed in high and lower points. Therefore, RES was measured in two different points of the fracture surfaces for this study.

A Point Load Testet equipment, PLT-100, was used to determine the rock embedment strength of some of the fracture surfaces before and after acid injection. A displacement gauge was attached to the equipment frame to measure an indentation distance equivalent to half of the radius of a steel ball of 0.0625 in. in diameter (Howard and Fast 1970). A pressure sensor included in the PLT-100 measures the load applied to

the steel ball. The configuration of the equipment made necessary to cut plugs from the cores used for acid injection. The plug dimensions were 1 in. in diameter and 2 in. long. An outline of the procedure to determine the rock embedment strength is presented below:

- Mark two measurement points on the plug surface.
- Place the plug in the bottom platen of the PLT-100.
- Position the steel ball on one of the measurement points.
- Push the “zero” button in the control box to reseal the load.
- Rise the bottom platen until the steel ball touched the top platen. This operation is done using a hydraulic loading jack attached to the equipment.
- Push the “zero” button to reseal the load in the control box.
- Record the distance showed in the displacement gauge. Add 0.016 inches to this distance (half of the radius of the steel ball). The total value is the final distance the lower platen has to be displaced.
- Continue rising the lower platen until reaching the final displacement distance.
- Record the load applied on the steel ball at this moment. The PLT-100 displays the load in kilo-newton.
- Open the valve of the hydraulic jack to lower the bottom platen.
- Position the steel ball in the second measurement point and repeat the procedure outline above. The second measurement is used to check the repeatability of the test.

- Calculate the RES using equation below:

$$RES = \frac{224.81 W}{\pi \left(\frac{d}{4}\right)^2} \dots\dots\dots(6)$$

Where RES is in psi, W is the load in kilo-newton, and d is the diameter of the projected area of indentation. d equals 0.0625 in. assuming that the area of indentation distance is equivalent to the cross sectional area of the steel ball.

2.2.4 Acid Injection

After the fracture surfaces are characterized, the cores are saturated in a vacuum vessel. After the saturation, the cores are ready for acid injection. The detailed procedure followed during acid injection is described below:

- Place Teflon tape around the core walls to prevent leaking. It is advised to wrap the core with Teflon tape only once at the top, middle, and bottom of the core walls. Apply vacuum grease (Dow Corn High Vacuum Grease) on the Teflon tape to secure it to the core walls for ease of installation.
- Fix the O-rings (251-VT90) inside the cell groove. Also, fix the O-rings in the cell caps (123-VT90) and pistons (351-VT90). The O-rings for the cell and caps should be changed after every acid injection. It is recommended to stretch out the cell O-rings before fixing them in the groove as well as applying glue in the groove to attach the O-rings and prevent their movement when placing the cores inside the cell.

- Apply O-ring grease (Dow Corn 55) on the cell and caps O-rings. For the pistons O-rings, use vacuum grease.
- Rest the conductivity cell vertically in the hydraulic table. Push the cores inside the cell and check that the direction of the arrows (direction of scanning) is pointing up and is the same for both cores.
- Use a shim (0.12 in. wide) to create an artificial fracture. Keep pushing the cores inside the cell until they touch the shim. Remove the shim.
- Remove the conductivity cell from the hydraulic table and place it on the crane table. Push the caps inside the lateral openings and fix them to the cell by tightening the bolts. To operate safely, screw a pair of metal rings on the top of the cell and use them to lift the cell with the crane.
- Screw the nuts in the tubing fittings of the cell caps to protect them during the transfer of the cell assembly.
- Place the cell back in the hydraulic table using the crane. Insert the pistons inside the cell slowly. Once the pistons contact the back of the core, stop pushing them and check the fracture width.
- Lock the hydraulic jack and screw the fittings in the front cell and pistons.
- Remove the nuts and connect the inlet and outlet flow lines to the cell caps. Also, connect the leak-off lines (pistons), the cell pressure line, and the fracture pressure differential lines.

- Connect the thermocouples in the inlet and outlet lines. In the inlet line, connect the thermocouple to the portable thermometer. In the outlet line, connect the thermocouple to the temperature controller.
- Cover the cell with the heating jacket and connect it to the temperature controller. Set up the temperature of the heating jacket to 250 °F for high temperature experiments and 170 °F for low temperature experiments. Preheat the cell for 1-2 hours before acid injection.
- Open the leak-off valve.
- Fill up the brine/water tank.
- Open the valve between the brine/water tank and as well as the valve in the line between the pump and the cell inlet.
- Close the valve between the acid tank and pump.
- Turn the pump on and start flowing water through the system at normal pump capacity.
- Set up the temperature controller in the cell outlet 2 °F below the temperature of study. It was observed that the exothermic reaction between HCl and calcite releases enough heat to increase the outlet temperature in 2 °F.
- Prepare the acid fluid. For gelled acids, use a shaft mixer while adding water, corrosion inhibitor, HCl and iron control agent. When the polymer is added, turn on the magnetic stirrer at medium speed to increase the mixing power in the tank.
- Keep mixing the acid for 30 minutes at high speed to allow for proper hydration of the polymer.

- Measure linear gel viscosities in the Fann 35A viscometer after 30 minutes of hydration. This is a control point to know if the polymer was hydrated correctly.
- Once the system reaches the set-point temperature, open the program Acid Frac Injection ERG.vi for recording data in Labview. A user manual for this program is included in Appendix A.
- Start increasing the cell pressure and leak-off back-up pressure in increments of 50 psi. Check for leaks in the system during each ramp.
- Increase the cell pressure up to 1000 psi and the leak-off pressure up to 980 psi. If the system does not have leaks, a constant differential pressure of 20 psi will be kept during the acid injection, except when acid breaks through the cores.
- Measure the flow rate in the cell outlet. It must be 1 liter per minute at 95% of the pump capacity in order to proceed.
- Place the outlet hose into the spent acid tank. While heating up the system with water, the hose can be resting in the sink.
- Open the valve between the acid tank and the pump while simultaneously closing the valve from the water tank.
- Open the check point valve located at the cell inlet very slowly. Use a pH strip to measure the pH of the fluid. Once the pH drops, start counting the rock-acid contact time.
- Measure and record the leak-off volumes every minute while the acid is pumped.
- Monitor and record the temperature of the inlet and outlet cell lines.
- Change the flow from acid to water once the rock-acid contact time is completed.

- Turn off the temperature controllers and start reducing the pressure in the cell and leak-off lines slowly.
- Monitor the pH of the fluids coming out of the cell. Keep flushing the system until the cell effluent pH increases to 7.
- Once the system has cooled down and the cell effluent has neutral pH, remove the heating jacket and turn the pump off.
- Open the hydraulic jack and disconnect the lines.
- Remove the front fittings and cover the inlet and outlet cell fittings with nuts.
- Lift the cell using the crane and place it on the table. Remove the pistons and caps.
- Rest the cell in the hydraulic table and remove the cores from the cell using the Teflon blocks.
- Remove the Teflon tape from the core walls and rinse the fracture surface.
- Scan the cores with the profilometer.
- Clean every component of the cell.

2.2.5 Acid Fracture Conductivity Measurements

Once the cores are scanned after acid injection, they are positioned back in the conductivity cell for the conductivity measurements. The process of fixing the O-rings and assembling the cell (caps and pistons) is the same as describe in the previous section. However, for conductivity measurements the fracture surfaces are placed in

contact to each other instead of leaving a space or fracture between them as with the acid injection step.

After assembly is complete, the cell is placed in a load frame with the help of the crane. A description of conductivity equipment and calculations are presented below:

- Place the cell horizontally in the center of the load frame. The direction of the water flow must be opposite to the acid injection direction.
- Apply a minimal pressure on the cell pistons in order to secure the cell in the load frame.
- Connect the inlet and outlet lines to the cell.
- Install the fittings in the cell body and pistons.
- Use nuts to plug the fittings in the pistons throughout the conductivity measurements. Pressure drop across the cores is not measured for conductivity; only pressure drop across the fracture is measured.
- Install the thermocouple in the outlet line and connect it to the portable thermometer readout.
- Connect the flow lines from the cell ports/fitting to the pressure transducers. Usually, the lowest range transducer (0-10 psi) is suitable for initial measurements at low closure stress levels.
- Lubricate the hose in the peristaltic pump. Use a generous amount of tube lube on the hose and pump rods.
- Open the inlet valve and close the outlet valve.

- Turn on the peristaltic pump at low speed. Cell pressure has to build up and reach a constant value. If the pressure does not build up, the system has a leak and it is necessary to disassemble the cell and repeat the previous procedure.
- Open the outlet valve and bleed the lines. This is a very important step to remove air trapped in the system.
- Open the Labview program: Acid Frac Conductivity ERG.vi. A description of how to use this program is presented in Appendix A.
- Regulate the pump speed and record the flow rate. In conductivity measurements, flow rate values are not scaled down from field conditions. Therefore, any value of flow rate is fine as it is kept constant for a given closure stress.
- Record the lowest pressure drop (ΔP_{min}) and highest pressure drop (ΔP_{max}) observed, cell pressure, and temperature. Although conductivity measurements are done at room temperature, temperature variations are used to calculate the water viscosity (μ_w).
- Replace q_w , ΔP , and μ_w values in Eq. 7 to calculate fracture conductivity. Maximum conductivity is calculated by replacing ΔP by ΔP_{min} . Minimum conductivity is calculated by replacing ΔP by ΔP_{max} .

$$k_{fw} = 26807.3 \left(\frac{q_w \mu_w}{\Delta P} \right) \dots \dots \dots (7)$$

Where k_{fw} is fracture conductivity in md-ft, q_w is the water flow rate in l/min minute, μ_w is the water viscosity in cP, and ΔP is the pressure drop across the fracture in psi. Derivation of Eq. 5 is explained in Appendix B.

- Calculate an arithmetic mean between the minimum and maximum value of conductivity found. This is the average conductivity.
- After 30 minutes of the first measurement, record flow rate, pressure drop (minimum and maximum) and calculate water viscosity if temperature varied. Calculate maximum, minimum, and average conductivity again.
- Repeat this procedure every 30 minutes until pressure drop across the fracture reaches a stable value.
- Raise the closure stress in increments of 500 psi. Repeat the procedure mentioned above until reaching stable pressure drop for each closure stress.
- Report the conductivity for each closure stress as the average conductivity yielded when the pressure drop reaches a constant value.
- Connect the lines to the next pressure transducer in range (0-30 psi) if the pressure drop value is higher than 10 psi. Bleed the lines to remove the air trapped before calculating conductivity again.
- Stop measuring fracture conductivity if the values calculated are on or below the matrix conductivity value $(k_{fw})_m$. Calculation of the matrix flow conductivity is presented in Appendix B.

- Turn off the peristaltic pump, reduce the closure stress slowly to zero, and disconnect the flow lines.
- Remove the cell from the load frame using the crane.
- Disassemble the cell (piston and caps) and remove the cores from the cell using the hydraulic table

2.3 Experimental Design

As mentioned in the project goals section, the objectives of this research work is to examine conditions that affect acid fracture conductivity by studying different levels of temperature, rock-acid contact time, and initial fracture surface as shown in **Table 1**:

Variable	Values
Temperature (°F)	100
	130
Rock-acid Contact Time (min)	5
	10
Initial Condition of Fracture Surfaces	Smooth
	Rough (Tensile Fractured)

Table 1—Experimental design.

Formation cooling effects during acid injection were considered to estimate the temperatures in which the experiments were conducted. In Table 1, the temperature values correspond to injection temperatures of the acid at the bottom hole instead of reservoir temperatures. These were calculated with Ramey's equations for heat transfer

in wellbores (Ramey, H.J 1962). The low and high temperature values in Table 1 correspond to the bottom and top of the production interval for the Austin Chalk formation respectively. The overall production interval for this formation ranges from 6900 to 11500 ft TVD (Martin et al. 2011). Additional parameters used for the injection temperatures calculations are shown in **Table 2** :

Parameter	Values
Geothermal Gradient (°F/ft)	0.01
Injection rate (bbb/min)	20
Surface Temperature (°F)	90
Linear Gel Acid Viscosity (cP)	50

Table 2—Parameter values used in Ramey’s equations.

Two values of rock-acid contact times, 5 and 10 minutes, were included in the experimental design. These contact times represent current acid injection times during multi-stage acid fracturing treatments in horizontal wells. Finally, two types of fracture surfaces, smooth and rough, were used to investigate if there is substantial difference between the values of conductivity measured for both types of surfaces at the same experimental conditions.

CHAPTER III

RESULTS AND DISCUSSION

According to the experimental design presented in the previous chapter, eight tests compound the experimental matrix. However, fifteen experiments were conducted in total; ten were successfully completed while five had to be stopped during the acid injection or conductivity measurements. Most of the problems were due to the lack of adherence of the silicon mix on the core walls. This caused the breaking of the coating when the cores were inserted inside the conductivity cell, during acid injection, or when closure stress was increased. The adherence problem was addressed by extending the sitting time of the silicon mix as explained in Chapter II. The successful experiments account for two experiments intended to check the repeatability of the experimental set up. The following sections present a basic petrophysical characterization of the Austin Chalk cores, experimental results and discussion, and a comparison of the experimental data with the correlation of Nirode and Kruk for acid fracture conductivity.

3.1 Basic Petrophysical Characterization of the Austin Chalk Cores

The permeability of several core samples was measured in the conductivity cell by flowing water through the bottom core and measuring the pressure drop at a constant flow rate. The permeability varied from 2.1 to 5.4 md. Porosity was also measured, ranging from 0.21 to 0.25. The Unconfined Compressive Strength (UCS) was provided by the cores vendor, being equal to 3500 psi. These results are shown in **Table 3**:

Property	Values
Permeability (md)	2.1-5.4
Porosity	0.21-0.25
UCS (psi)	3500

Table 3—Basic petrophysical characterization of the Austin Chalk cores.

Young's modulus and Poisson ratio were measured following a multiple-stage triaxial test procedure at room temperature and with an axial strain rate of 0.03%/minute.

The results are summarized in **Table 4**.

Confining pressure (psi)	Young's modulus (psi)	Poisson ratio
80	1.45E+06	0.117
1000	2.37E+06	0.007
3000	2.35E+06	0.068

Table 4—Young modulus and Poisson ratio of Austin Chalk cores.

3.2 Experimental Results and Discussion

In order to facilitate the discussion, this section presents the experimental results classified by low and high temperature levels, 100 and 130 °F, respectively. The results encompass the etched fracture surfaces profiles, V_{etched} values, and the curves of acid fracture conductivity against closure stress for the different experimental conditions. For visual purposes, only the etched profiles of the bottom cores are shown in this chapter. The etched profiles of the top cores are shown in Appendix C.

3.2.1 Low Temperature Level

Linear gelled acid was pumped at 100 °F in six experiments. Two of those experiments were conducted with cores having rough fracture surfaces. The remaining four experiments were done with smooth fracture surfaces cores. For one experiment with rough fracture surfaces, acid was pumped for 5 minutes while for the experiment acid was pumped for 10 minutes. For the smooth cores, acid was pumped for 5 minutes in two pairs of cores, being the second pair a duplicate to check for repeatability in the experimental set up. Likewise, acid was pumped for 10 minutes in two pair of smooth cores, being the second pair a repetition.

The etched profiles for the smooth fracture surfaces after 5 and 10 minutes of rock-acid contact are shown in **Fig. 18**. The red tones in the color scale represent shallow depths. As moving down in the scale, the colors palette represents larger depths.

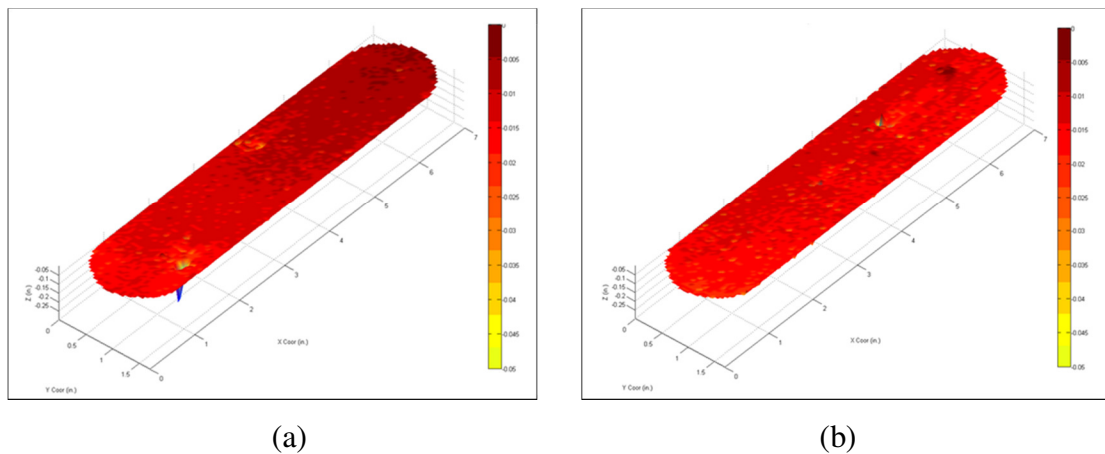


Fig. 18—Etched fracture surfaces of smooth surface cores. (a) 5 minutes of rock-acid contact at 100 °F, (b) 10 minutes of rock-acid contact at 100 °F.

Both profiles feature the creation of roughness on the fracture surfaces after acid reaction. Some large wormholes were created while small wormholes predominate. The color scale also shows more rock dissolution for 10 minutes than 5 minutes of acid injection. In volumetric values, V_{etched} was 0.131 in³ for 5 minutes and 0.151 in³ for 10 minutes.

Fig. 19 presents the rough fracture surface before and after 5 minutes of rock-acid contact. The acid dissolved the high points and enlarged the deeper zones on the fracture surface. The same type of dissolution but in larger magnitude was observed in the experiment using rough fracture surfaces and injecting acid for 10 minutes as shown in **Fig. 20**. The acid dissolved the high points and enlarged the deeper zones on the fracture surface. For both rough fracture surface experiments, the wormholes sizes were smaller compared to the wormholes observed in the smooth fracture surface experiments at 100 °F.

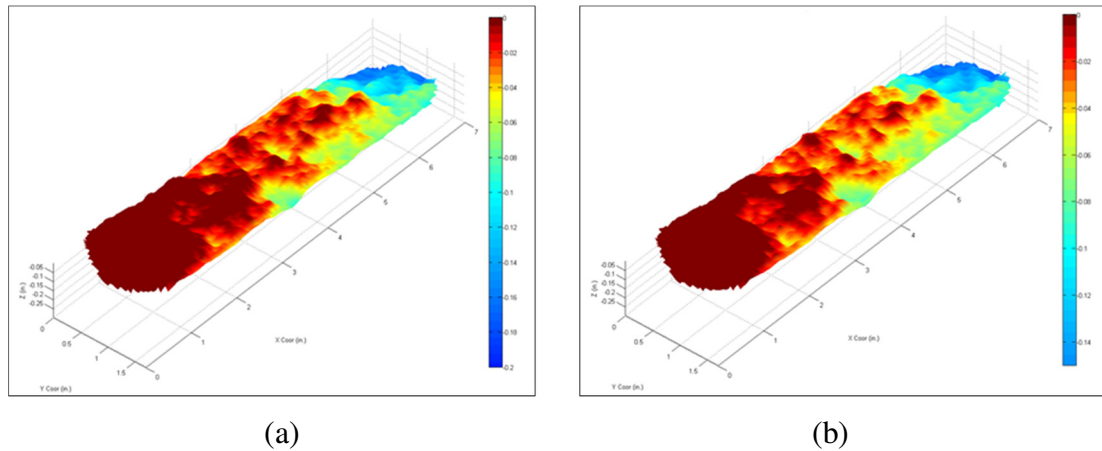


Fig. 19—Fracture surfaces of rough surface core. (a) Before acid injection, (b) After 5 minutes of rock-acid contact at 100 °F.

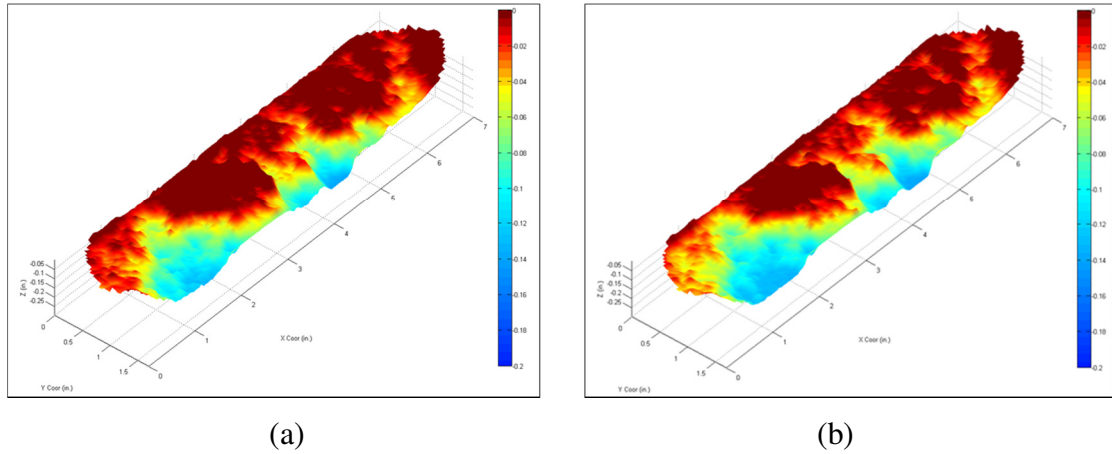


Fig. 20—Fracture surfaces of rough surface core. (a) Before acid injection, (b) After 10 minutes of rock-acid contact at 100 °F.

The volumes of rock dissolved by the acid (V_{etched}) for the rough fracture surface experiments as well as for the smooth ones are summarized in the **Table 5**. As expected, larger rock-acid contact times yields to higher V_{etched} values. On the other hand, the values of V_{etched} for experiments using rough fracture surfaces were smaller than for smooth fracture surfaces. This phenomenon points out differences in the rock dissolution for each type of fracture surface.

Fracture Surface	Rock-Acid Contact Time (minutes)	V_{etched} (in ³)
Smooth	5	0.131
	10	0.151
Rough	5	0.062
	10	0.103

Table 5—Summary of V_{etched} values for experiments at 100 °F.

The acid fracture conductivity curves for the experiments conducted at 100 °F are shown in **Fig. 21**. The dashed line represents the value of matrix conductivity determined for Austin Chalk. Three trends of fracture conductivity decline were identified for all the experiments. 68% of fracture conductivity generated by acid etching was lost from 0 to 500 psi. Then fracture conductivity decreased with closure stress at a slower rate until 2500 psi. From that point, the continuous increment of closure stress caused a second rapid decline of the fracture conductivity until matrix conductivity was reached at 3500 psi of closure stress.

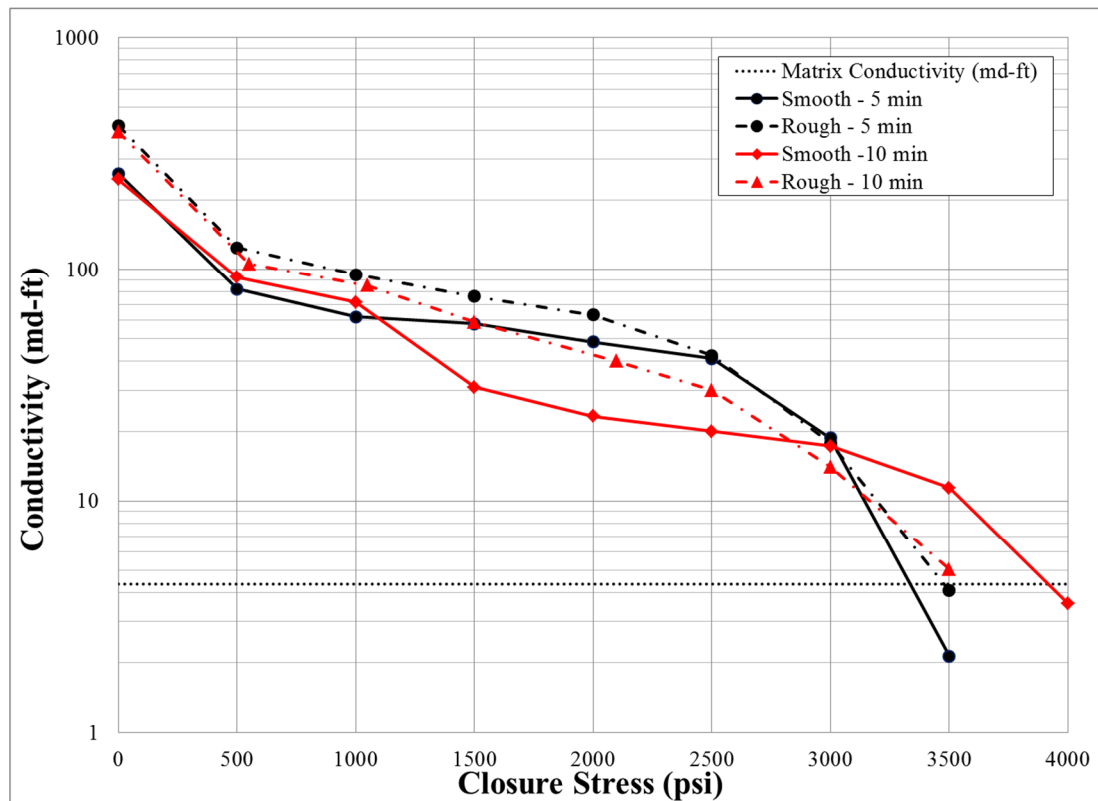


Fig. 21—Acid fracture conductivity for experiments at 100 °F

One of the major findings extracted from Fig. 21 was the observation of no significant difference in fracture conductivity at high closure stress for the experiments conducted at the same experimental conditions but using either smooth or rough fracture surfaces. Even though the volumes of rock dissolved by the acid were larger in the smooth fracture surfaces, their fracture conductivity was not higher than the values measured for rough surfaces.

From Fig. 21, the role of the rock strength after acid injection can be analyzed as well. Comparing the fracture conductivity curves of the rough fracture surfaces (dashed lines), they almost overlap at low levels of closure stress. However, the fracture surfaces exposed to acid for less time retained higher fracture conductivity when increasing the closure stress. A similar behavior was observed when the fracture conductivity curves of the smooth surfaces were compared (solid lines). Rock embedment strength measurements were done on fracture surfaces before and after injecting acid for 5 and 10 minutes at 100 °F. The results are summarized in **Table 6**. Higher contact times deteriorated the formation strength, negatively affecting the fracture conductivity for the experiments where acid was pumped for 10 minutes.

Rock-Acid Contact Time (minutes)	Rock-Acid Contact Time (minutes)		Strength Reduction (%)
	Before Acid	After Acid	
5	6988.2	6149.6	12.0
10	8385	5590.5	33.3

Table 6—Summary rock embedment strength values for experiments at 100 °F.

3.2.2 High Temperature Level

Linear gelled acid was injected in four pairs of cores at 130 °F in four experiments. For two experiments, the rock-acid contact time was 5 minutes in smooth and rough fracture surfaces. For the remaining two experiments, acid was pumped for 10 minutes for both types of fracture surfaces as well.

The profiles of the smooth fracture surfaces after injecting acid for 5 and 10 minutes at 130 °F are presented in **Fig. 22**. As observed at the lower level of temperature, these etched profiles also feature the creation of roughness on the fracture surfaces after acid reaction. V_{etched} were 0.135 in³ for 5 minute and 0.175 in³ for 10 minutes. As expected, the rock dissolution was higher at the longest rock-acid contact time.

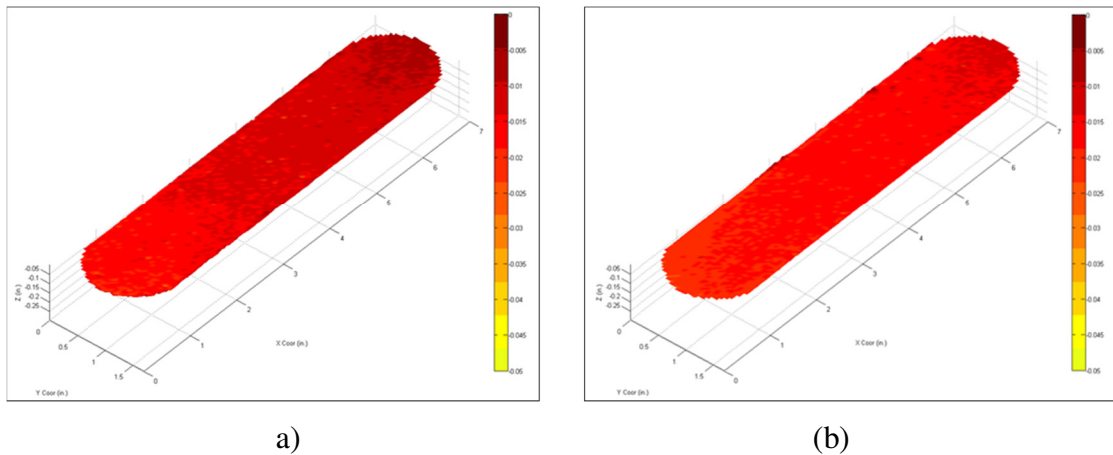


Fig. 22—Etched fracture surfaces of smooth surface cores. (a) 5 minutes of rock-acid contact at 130 °F, (b) 10 minutes of rock-acid contact at 130 °F.

Fig. 23 shows the rough fracture surface before and after 5 minutes of rock-acid contact. V_{etched} was 0.082 in³. The acid smoothed the high points and enlarged the deeper

zones on the fracture surface. This mechanism of rock dissolution was similar as the observed for the experiments at 100 °F.

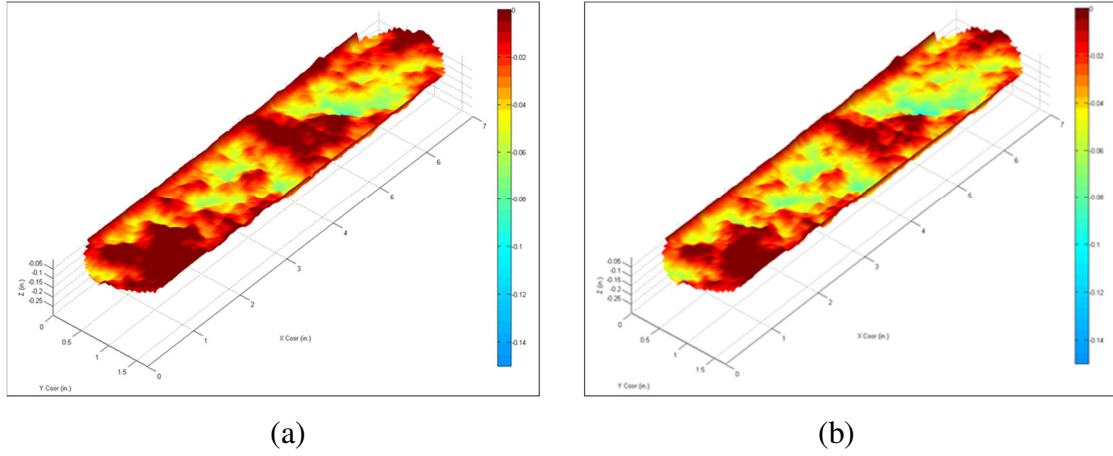


Fig. 23—Fracture surfaces of rough surface core. (a) Before acid injection, (b) After 5 minutes of rock-acid contact at 130 °F.

Fig. 24 shows the rough fracture surface before and after 10 minutes of rock-acid contact. For this experiment, the acid also smoothed the original features of the fracture surface. At these conditions, V_{etched} was 0.144 in^3 . This value is 43% higher than the one measured after 5 minutes of acid injection. The occurrence of wormholes in both experiments using rough surfaces was less than the ones observed in smooth surfaces.

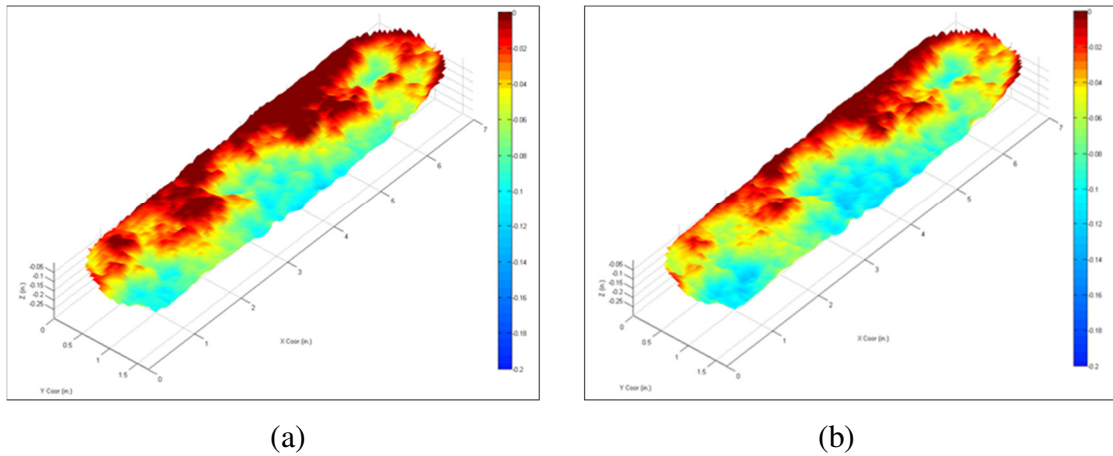


Fig. 24—Fracture surfaces of rough surface core. (a) Before acid injection, (b) After 10 minutes of rock-acid contact at 130 °F.

The volumes of rock dissolved by the acid for the rough and smooth fracture surface experiments at 130° F are summarized in the **Table 7**. Larger rock-acid contact times yielded to higher V_{etched} values. Likewise, the increment in temperature generated higher V_{etched} values. As observed for the experiments at 100 F, the rock dissolution in rough fracture surfaces were smaller than for smooth fracture surfaces at 130 °F. The acid fracture conductivity curves for the experimental conditions studied at 130 °F are shown in **Fig. 25**.

Fracture Surface	Rock-Acid Contact Time (minutes)	V_{etched} (in ³)
Smooth	5	0.135
	10	0.175
Rough	5	0.082
	10	0.144

Table 7—Summary of V_{etched} values for experiments at 130 °F.

Higher volumes of rock dissolved due to the increment of temperature yield a higher conductivity values when compared to the experiments conducted at 100 °F. The fracture conductivity decline for these curves featured a first trend up to 2000 psi and after that a steeped decline until matrix conductivity was reached at 3500 psi of closure stress. No significant difference was observed between experiments using rough and smooth fracture surface at the same experimental conditions. The large volumes of rock dissolved by the acid in smooth fracture surfaces did not contribute to generate higher conductivity values than the ones measured for rough fracture surfaces experiments.

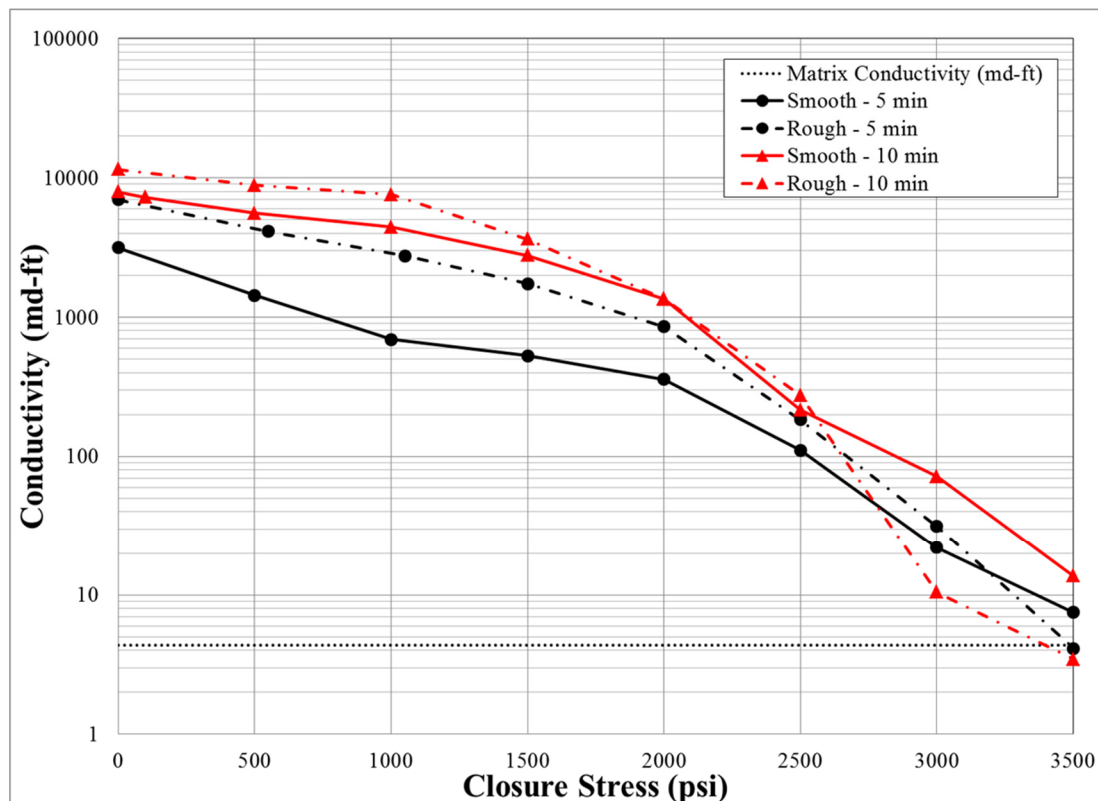


Fig. 25—Acid fracture conductivity for experiments at 130 °F.

Rock Embedment Strength measurements were performed on fracture surfaces before and after injecting acid for 5 and 10 minutes at 130 °F. The results are presented in **Table 8**. Strength reduction was higher on fracture surfaces that were in contact with acid for longer time (10 minutes-red line compared to 5 minutes-black line). However, these fracture surfaces were able to hold higher conductivity when compared to the experiments with 5 minutes of acid injection.

Rock-Acid Contact Time (minutes)	Rock-Acid Contact Time (minutes)		Strength Reduction (%)
	Before Acid	After Acid	
5	6988.2	6149.6	12.0
10	7826.8	5590.5	28.6

Table 8—Summary rock embedment strength values for experiments at 130 °F.

3.2.3 Experimental Results vs. Nirode & Kruk Correlation

The acid fracture conductivity results discussed in the previous sections were compared to the predictions of Nirode and Kruk’s correlation for fracture conductivity presented in Chapter I. It is important to mention that the experimental set up and equipment used in this research work is different from the apparatus used by Nirode and Kruk in 1973. The main differences are related to the core dimensions and geometry, acid injection rates and the acid-leak off. Nirode and Kruk used core plugs of 1-in. diameter and 2-3 in. long. In addition, the acid was injected at matrix flow without leak-off.

In general, the experimental data presented large discrepancy with the values predicted by Nirode and Kruk's correlation. However, specific differences were noticed in function of the acid injection temperature. For the experiments conducted at 100 °F, the initial values of conductivity had agreement until 500 psi of closure stress. After that, the divergence increased between the experimental data and the correlation predictions. The experimental data suggests that the loss of conductivity is not abrupt but it gradually declines. Contrary, the correlation predicts a steeped decline on conductivity which is driven by the low value of rock embedment strength measured for the Austin Chalk cores. **Table 9** shows a compilation of the comparisons for all the experiments conducted at 100 °F.

The results for the experiments at 130 °F presented large discrepancy with the correlation predictions along the entire range of closure stress applied as shown in **Table 10**. For all the experiments, the initial values of conductivity measured were higher than the values predicted by the correlation. Nirode and Kruk's correlation calculates the initial fracture conductivity value based on the ideal fracture width. The discrepancy with the experimental data may be due the differential acid etching that generated higher values of fracture width at zero closure stress. For the remaining range of closure stress, the correlation predicts a rapid decline of fracture conductivity while the experimental data shows a different decline trend and moreover slower conductivity reduction. This points out that even having low rock strength, Austin Chalk formation can retain higher values of fracture conductivity than those predicted by Nirode and Kruk's correlations. .

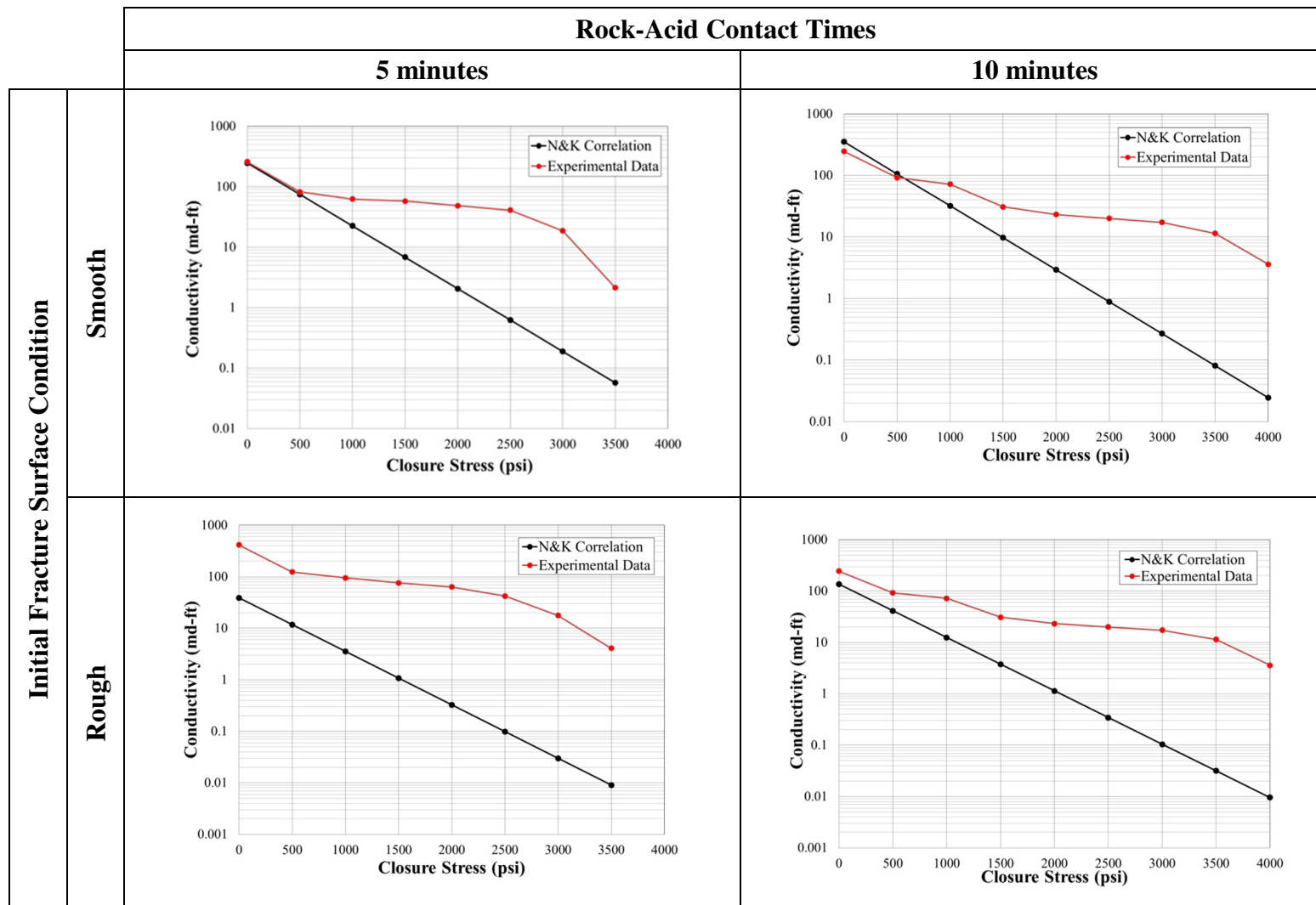


Table 9—Acid fracture conductivity results at 100 °F compared to Nirode and Kruk correlation.

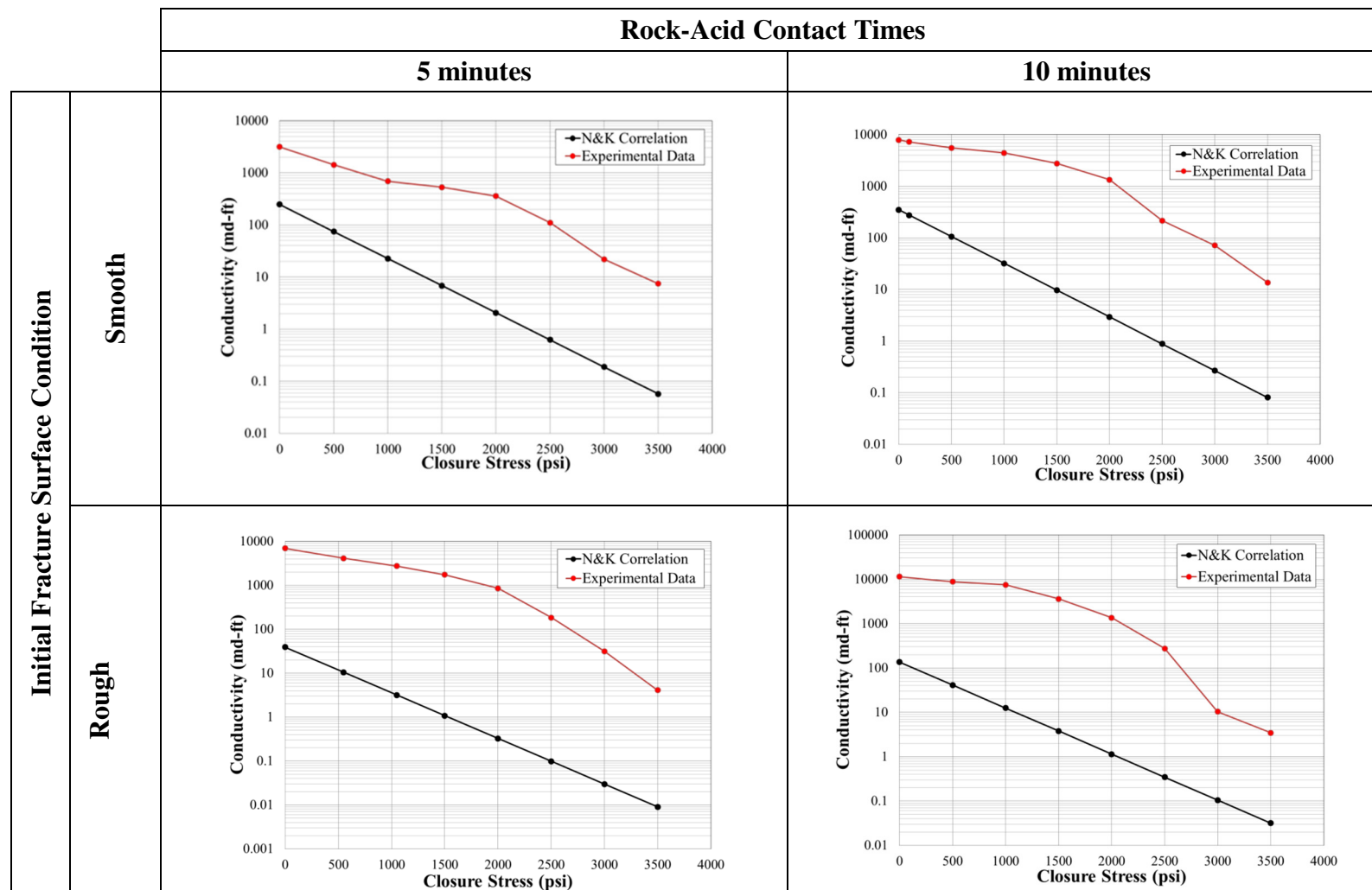


Table 10—Acid fracture conductivity results at 130 °F compared to Nirode and Kruk correlation.

CHAPTER IV

CONCLUSIONS AND RECOMMENDATIONS

4.1 Conclusions

Based on the experimental study, the following conclusions were established:

- The volume of rock dissolved by the acid was larger in smooth fracture surfaces than in rough fracture surfaces. This points out differences in the rock dissolution for each type of fracture surface.
- Although the volumes of rock dissolved by the acid were larger in smooth fracture surfaces than in rough ones at both temperatures of study, this did not yield to higher values of fracture conductivity. No significant difference in acid fracture conductivity was observed between experiments using rough and smooth fracture surface at high closure stress at the same experimental conditions.
- Mixed results were found between fracture conductivity and weakening of the rock strength after acid injection. While in the low acid injection temperature, the fracture conductivity was less for the experiments that had higher rock embedment strength reduction, for the high injection temperature the weakening of the rock strength did not negatively affect the fracture conductivity values.
- The mechanism of conductivity creation in smooth surfaces seems connected to uneven etching of the rock and roughness generation.
- For rough surfaces, acid conductivity is more related to the smoothness of peaks and their mismatch as the fracture closes than by asperities or roughness creation.

- Large disagreement was found in fracture conductivity between the experimental results and the predictions using Nirode-Kruk correlation. The discrepancy is due to the low formation strength of Austin Chalk which causes a drastic reduction of conductivity as closure stress increases in the correlation. Our experimental data showed that the conductivity reduction might not be as steep as predicted by the correlation. Even though the Austin Chalk is a soft rock, this may provide sufficient fracture conductivity at high closure stress.

4.2 Recommendations

This study performed acid injection at constant leak-off pressure. It would be interesting to investigate the effect that variation of leak-off pressure with time has on acid fracture conductivity. The pressure response of the fracture and leak-off during acid injection can be simulated with a pressure leak-off profile as described by Pongthunya (2007).

Regarding the difference in volumes of rock dissolution between smooth and rough fracture surfaces, a more detailed study is needed to investigate the effects that the fracture surface shape have on the reaction kinetics and diffusivity coefficients of the rock/acid system.

Finally, further experimentation with different formation types is necessary to establish the ranges of formation strength which would yield to different fracture conductivity values between smooth and rough fracture surfaces.

REFERENCES

- Anderson, M.S. and Fredrickson, S.E. 1989. Dynamic Etching Test Aid Fracture-Acidizing Treatment Design. *SPE Production Engineering* **4** (4): 443-449. SPE-16452-PA. <http://dx.doi.org/10.2118/16452-PA>.
- Antelo, L.F., Pournik, M., Zhu, D., et al. 2009. Surface Characterization and its Effect on Fracture Conductivity in Acid Fracturing. Paper SPE 119743 presented at the SPE Hydraulic Fracturing Technology Conference, The Woodlands, Texas, 19-21 January. <http://dx.doi.org/10.2118/119743-MS>.
- API RP-61, Recommended Practices for Evaluating Short Term Proppant Pack Conductivity, first edition. 1989. Washington, DC: API.
- Beg, M.S., Kunak, A.O., Gong, M., et al. 1998. A Systematic Experimental Study of Acid Fracture Conductivity. *SPE Production & Facilities* **12** (4): 267-271. SPE-52402-PA. <http://dx.doi.org/10.2118/52402-PA>.
- Broadbent, G.C., Knox, J.A. and Fredrickson, S.E. 1968. Dynamic Etching Tests and Their Use in Planning Acid Treatments. Paper SPE 2362 presented at the Oklahoma Regional Meeting of the Society of Petroleum Engineers of AIME, Stillwater, Oklahoma, 25 October. <http://dx.doi.org/10.2118/2362-MS>.
- Crowe, C.W. 1987. Principles of Acid Fracturing. In *Reservoir Stimulation*, ed. Economides M.J. and Nolte K.G, Chapter 17, 10-12. Houston, Texas: Schlumberger Educational Services.
- Gomaa, A.M. and Nasr-El-Din, H.A. 2009. Acid Fracturing: The Effect of Formation Strength on Fracture Conductivity. Paper SPE 119623 presented at the SPE Hydraulic Fracturing Technology Conference, The Woodlands, Texas, 8-10 June. <http://dx.doi.org/10.2118/119623-MS>.
- Grabski, Elizabeth. 2012. Matrix Acidizing Core Flooding Apparatus: Equipment and Procedure Description. MS thesis, Texas A&M University, College Station, Texas (August 2012).
- Howard, G.C and Fast, C.R. 1970. *Hydraulic Fracturing*. Vol. 2, 61-63, Dallas, Texas and New York: Monograph Series, SPE of AIME.
- Lund, K., Fogler, H.S., McCune, C.C., et al. 1975. Acidization-II. The Dissolution of Calcite in Hydrochloric Acid. *Chemical Engineering Science* **30** (8): 825-835. [http://dx.doi.org/10.1016/0009-2509\(77\)80003-1](http://dx.doi.org/10.1016/0009-2509(77)80003-1).

- Malagon Nieto, Camilo. 2007. 3D Characterization of Acidized Fracture Surfaces. MS thesis, Texas A&M University, College Station, Texas (May 2007).
- Martin, R., Baihly, J., Malpani, R., et al. 2011. Understanding Production from Eagle Ford-Austin Chalk System. Paper SPE 145117 presented at the SPE Annual Technical Conference and Exhibition, Denver, Colorado, 30 October -2 November. <http://dx.doi.org/10.2118/145117-MS>.
- Melendez, M.G., Pournik, M., Zhu, D., et al. 2007a. The Effect of Acid Contact Time and the Resulting Weakening of the Rock Surfaces on Acid Fracture Conductivity. Paper SPE 107772 presented at the SPE European formation Damage Conference, Scheveningen, The Netherlands, 30 May -1 June. <http://dx.doi.org/10.2118/107772-MS>.
- Melendez, M.G. 2007b. The Effects of Acid Contact Time and Rock Surfaces on Acid Fracture Conductivity. MS thesis, Texas A&M University, College Station, Texas (August 2007).
- Neumann, L.F. 2011. Experimental Investigation about the Generation, Visualization, Evaluation of Conductivity in Acidized Fractures in Microbial Carbonates (in Portuguese). MS thesis, Campinas State University, Campinas, Brazil (July 2011).
- Neumann, L.F., De Oliveira e Sousa, J.L.A., Brandao, E.M., et al. 2012. Acid Fracturing: New Insights on Acid Etching Patterns from Experimental Investigation. Paper SPE 152179 presented at the SPE Hydraulic fracturing technology Conference, The Woodlands, Texas, 6-8 February. <http://dx.doi.org/10.2118/152179-MS>.
- Nierode, D.E., Williams, B.B. and Bombardieri, C.C. 1972. Prediction of Stimulation from Acid Fracturing Treatment. *Journal of Canadian Petroleum Technology* **11** (4): 31-41. JCPT72-04-04. <http://dx.doi.org/10.2118/72-04-04>.
- Nierode, D.E. and Kruk, K.F. 1973. An Evaluation of Acid Fluid Loss Additives, Retarded Acids, and Acidized Fracture Conductivity. Paper SPE 4549 presented at 48th Annual Fall Meeting of the Society of Petroleum Engineers of AIME, Las Vegas, Nevada, 30 September-3 October.
- Pongthunya, Potcharaporn. 2007. Development, Set Up and Testing of a Dynamic Hydraulic Fracture Conductivity Apparatus. MS thesis, Texas A&M University, College Station, Texas (August 2007).
- Pournik, M., Zou, C., Malagon Nieto, M.G., et al. 2007. Small-Scale Fracture Conductivity Created by Modern Acid-Fracture Fluids. Paper SPE 106272

presented at the SPE Hydraulic Fracturing Technology Conference, College Station, Texas, 29-31 January. [http://dx.doi.org/ 10.2118/106272-MS](http://dx.doi.org/10.2118/106272-MS).

Pournik, Maysam. 2008. Laboratory-Scale Fracture Conductivity Created by Acid Etching. PhD dissertation, Texas A&M University, College Station, Texas (December 2008).

Pournik, M., Gomaa, A. and Nasr-El-Din, H.A. 2010. Influence of Acid-Fracture Fluid Properties on Acid-Etched Surfaces and Resulting Fracture Conductivity. Paper SPE 128070 presented at the SPE International Symposium and Exhibition on Formation Damage Control, Lafayette, Louisiana, 10-12 February. <http://dx.doi.org/10.2118/128070-MS>.

Ramey, H.J. 1962. Wellbore Heat Transmission. *Journal of Petroleum Technology* **14** (4): 427-435. SPE-96-PA. <http://dx.doi.org/10.2118/96-PA>.

Smith, C.F., Crowe, C.W. and Wieland, D.R. 1970. Fracture Acidizing in High Temperature Limestone. Paper SPE 2859 presented at the SPE Deep Drilling and Production Symposium, Monahans, Texas, 26 March. <http://dx.doi.org/10.2118/2859-MS>.

Yango, Takwe. 2011. Characterization of Filter Cake Buildup and Cleanup Under Dynamic Fluid Loss Conditions. MS thesis, Texas A&M University, College Station, Texas (August 2011).

Zhou, C. 2006. Development and Testing of an Advanced Acid Fracture Conductivity Apparatus. MS thesis, Texas A&M University, College Station, Texas (May 2006).

APPENDIX A

A.1. User guide for Profilometer and MATLAB processing .

A guide to use the profilometer and its code was written by Yango (2011) based on the work developed by Malagon (2007) which included the coding and building of the profilometer. The following user guide is based on Yango (2011).

Profilometer User Guide.

- Turn on the profilometer control box (switch is on box)
- Open the Labview program **profilomenter.vi** Fig. A-1

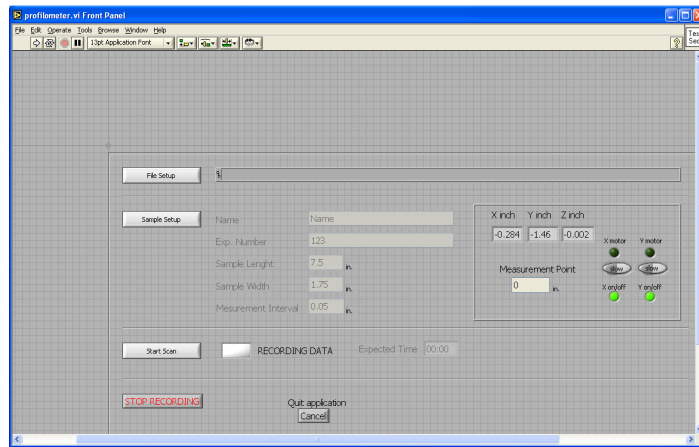



Fig. A-1—Profilometer controls input screen (before run button is clicked).

- Click the run button,  , symbol located at the top right of the screen

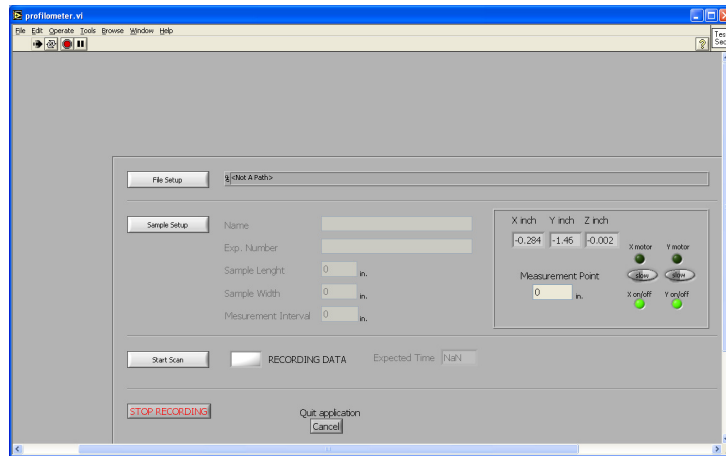



Fig. A-2—Profilometer controls input screen (after run button is clicked).

- Put the mode switches on the profilometer control box to manual and jog using the position buttons so that the X inch and Y inch coordinates are zero inches. You cannot adjust the Z position; it is read in from the laser.
- Click on **File Setup** then enter file name and location
- Click on **Sample Setup** and enter sample name, experiment number, sample length and measurement interval.
- For acid fracturing experiments, the following settings are recommended (to allow seamless data processing in the MATLAB code): *Sample Length*: 7 in., *Sample Width*: 1.7 in., and *Measuring Interval*: 0.05 in.
- Put the switches on the laser control box to Auto and click on **Start Scan**.

- Once recording is finished click on STOP RECORDING then click on the abort execution button, . The scanned file (*.dat) should now be saved in the user specified location.

Data Processing in Matlab

- Store labview files (*.dat) from section I in C:\Profiles.
- Open Matlab and load the program
AA_OringinalDataProccesorToMatLabFile_Original (file located in C:\profiles)
- In the Matlab editor, go to line 28 of the program and enter the file name of the file you want to convert from labview output to a matrix format to be read by Matlab.
- Hit the run button (green forward facing triangle) or go to *debug > Run*
AA_OringinalDataProccesorToMatLabFile_Original or just hit **F5**
- In the Matlab command window answer the prompts. Note: Enter zero for phase and no ('n') for inversion assuming you had the same starting reference point for the *before* and *after* scan.
- Processed data is saved to *C:\MLfiles\ProccesedData*

- To calculate volumes from difference in surfaces open *AA_Final_VolumeCalculator* (file located in C:profiles)
- On lines 41 and 42 of the editor, enter the names of the *before* and *after* files created from steps 4 and 5
- Click on run or hit F5.
- Charts are displayed to show surfaces and an ‘etched’ volume is given in the command window

The file paths stated below are default locations programmed in the original Matlab code. The user can change the locations in the code as desired.

Sample Chart

Following the above procedure with the provided files (*RS2B_After.dat* and *RS2B_Before.dat*) the following figure and etched volume are obtained:

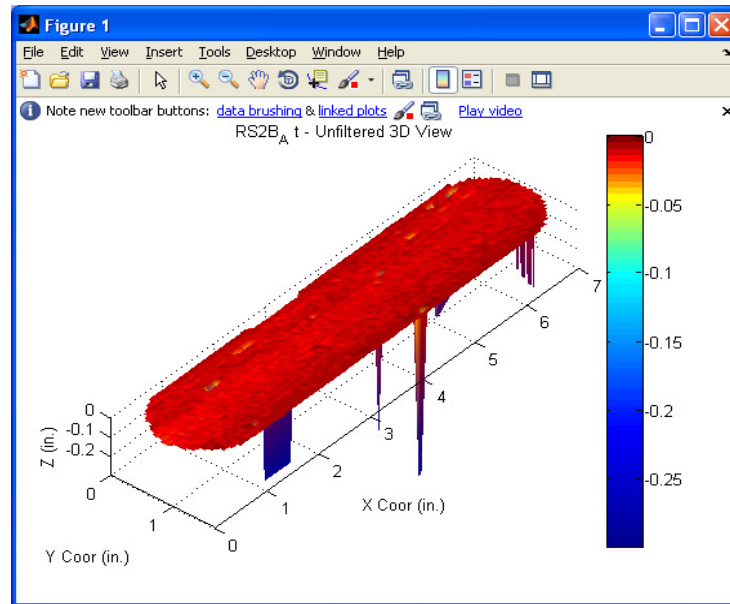


Fig. A-3—Surface plot for experiment RS2B.

Results as displayed in the MATLAB command window are presented below:

RS2B_A t

Phase Applied to the AFTER Sample: 0.0000 in.

Phase Applied to the BEFORE Sample: 0.0000 in.


Etched Volume: 0.160 in³

A.2. User Guide for Acid Injection and Fracture Conductivity Programs.

The object code in the programs for recording data during acid injection and fracture conductivity measurements was developed for matrix acidizing experiments by Grabski (2012) and adapted for acid fracture conductivity experiments. The code and

user interphase is the same for acid injection and acid fracture conductivity measurements.

Data Recording.

- Open the program **Acid Frac Injection ERG.vi** . The front panel, as shown in **Fig. A-4**, contains the displays of the cell pressure, pressure drop in the fracture and leak-off.

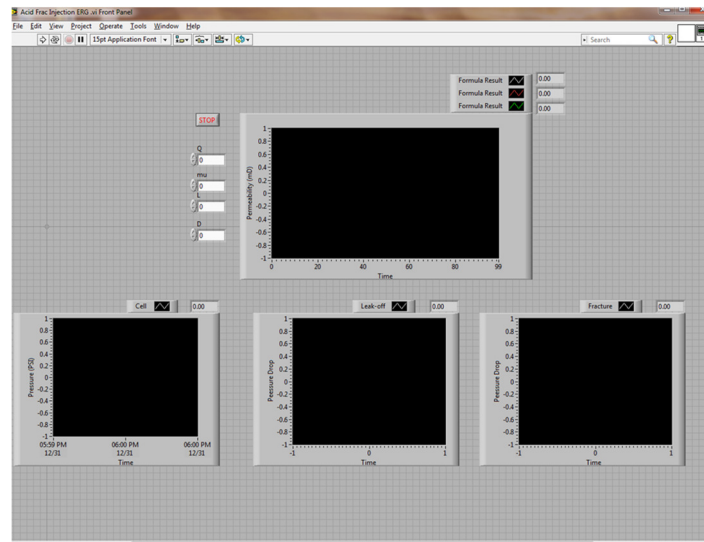


Fig. A-4—Front panel of Acid Frac Injection.vi.

The Fig. A-5 shows the front panel for the conductivity program Acid Frac Conductivity.vi.

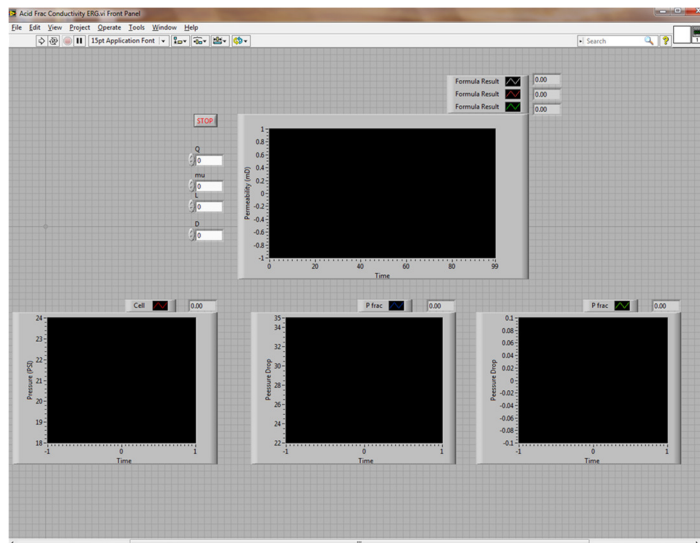


Fig. A-5—Front panel of Acid Frac Conductivity.vi.

- Select **Window** and then click **Show Block Diagram**.

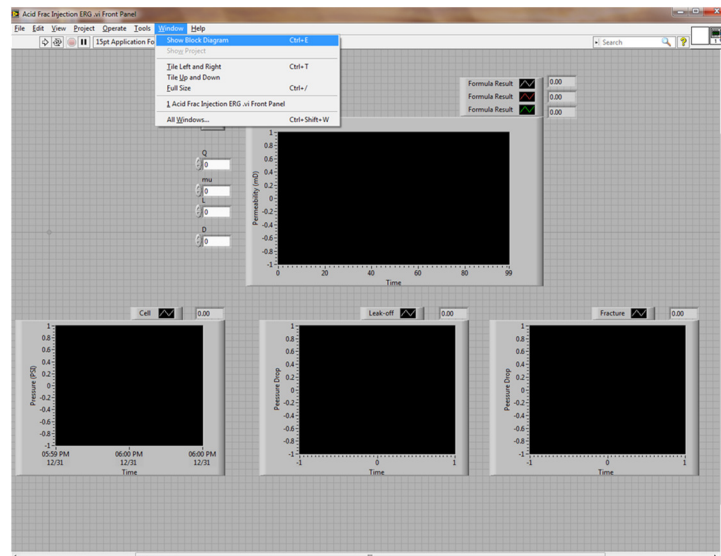


Fig. A-6—Selecting Show Block Diagram panel.

- Double-click **Write To Measurement File2** box on the block diagram panel.

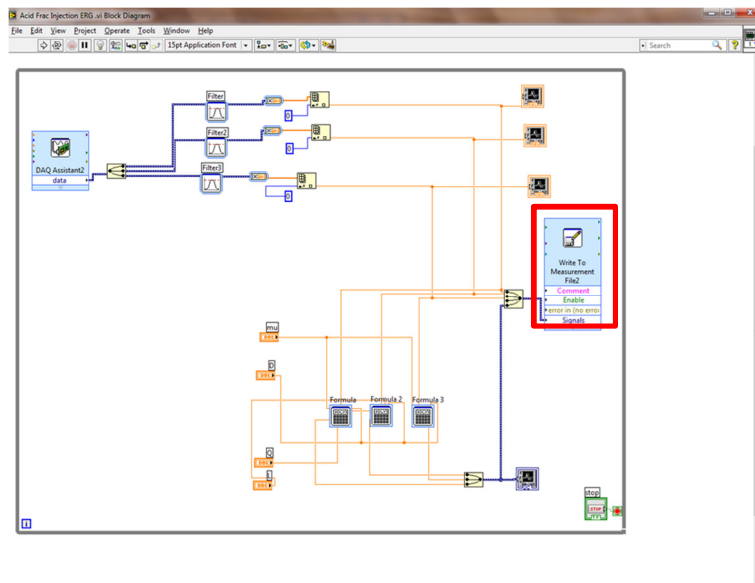


Fig. A-7—Opening object to save .lvm file.

- Select the file location and write the file name on the **File Name** box (e.g. TEST1.lvm). Then click **OK**.

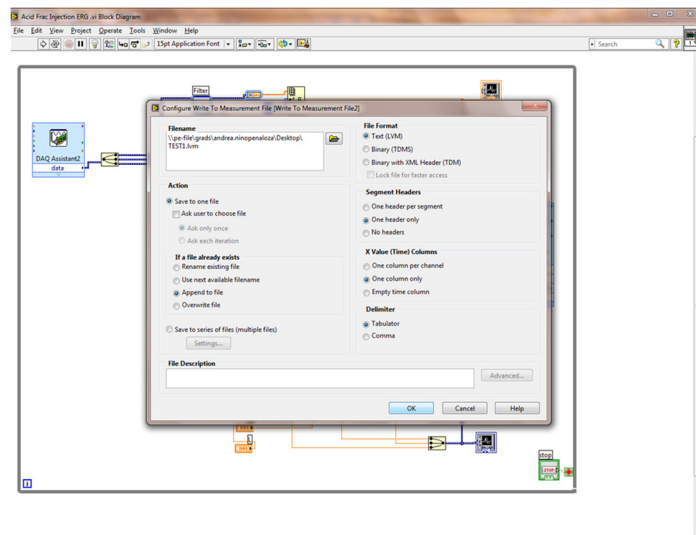


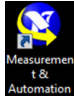


Fig. A-8—Saving .lvm files.

- Click **Window** and then select **Show Front Panel**
- Click the button **Run**, , to start recording data.
- Click the button **Stop**,
- , to stop recording data.
- Exit the program once the data recording is complete and click on **Do Not Save Changes** button.

Calibration of Pressure Transducers.

A description of the procedure to calibrate the pressure transducers used for acid injection and conductivity measurements is presented below. It is strongly advised to periodically calibrate them.

- Open the program **Measurements & Automation Explorer** 
- Double-click in **Devices and Interfases** to detect the Data Acquisition Card (DAC)
- Select the DAC installed. For this example, the DAC is called **NI PCI-6221** “**Dev 1**” as shown below:

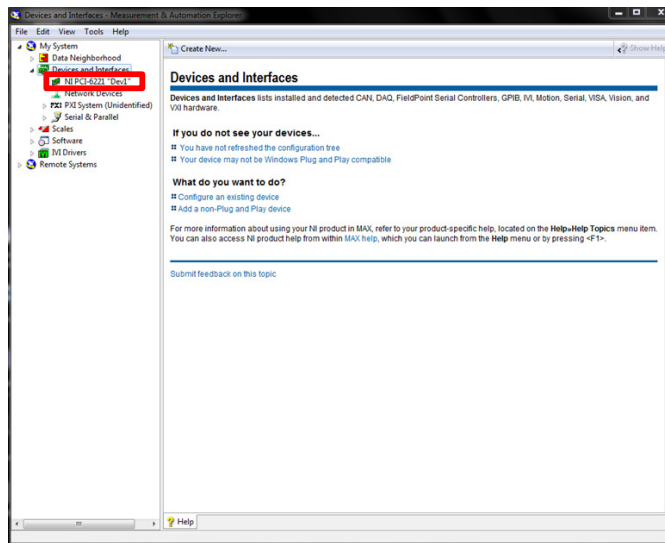


Fig. A-9—Detection DAC.

- Click **Test Panels** button and select the device (pressure transducer) you want to calibrate from the drop-down menu **Channel Name**. For this example, the device to calibrate is the pressure transducer Dev1/ai0 in the **Acid Fra Injection ERV.vi**.

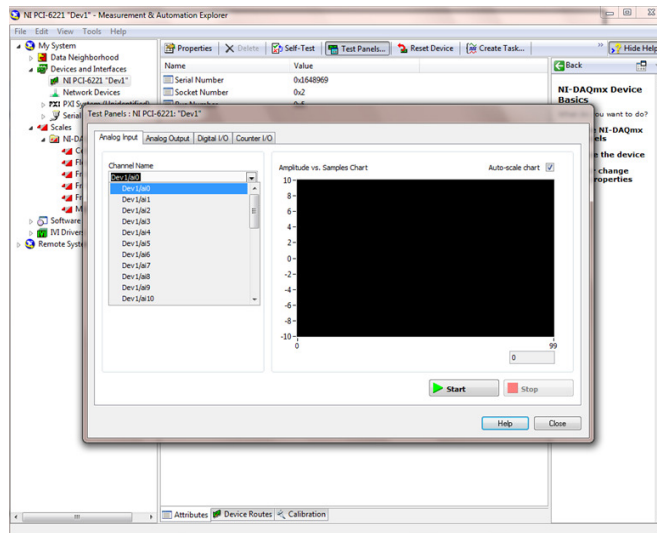



Fig. A-10—Selection of device to be calibrated.

- Release pressure in the transducer to reach 0 psi. This is the first point in the calibration line.
- Click start button, , to initiate the test of Dev1/ai0. The voltage amplitude should be between 1.3 to 1.44 volts.

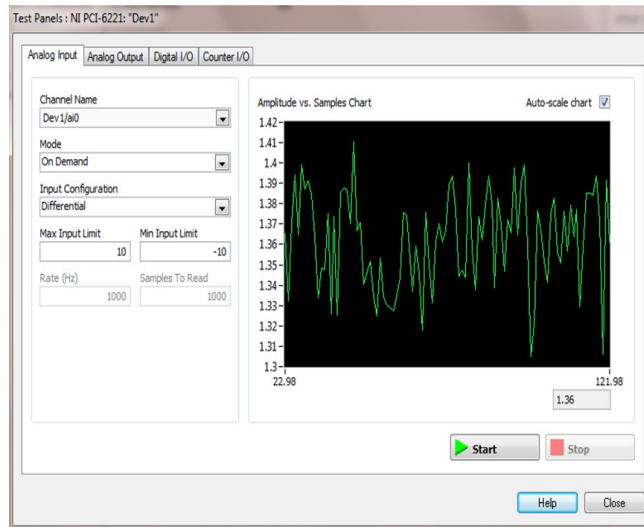



Fig. A-11—Testing device for 0 psi. Initial point.

- Take an average from the oscillating values and assign 0 psi to this voltage value.
- Click stop button, .
- Increase the pressure in the transducer. This is the second point in the calibration line. It is advisable to raise the pressure up to maximum value for which the transducer was originally calibrated in the factory.
- Click the start button and take a volt average value corresponding to the pressure.
- Calculate the slope and intercept by doing a linear regression between the first and second point of the calibration.

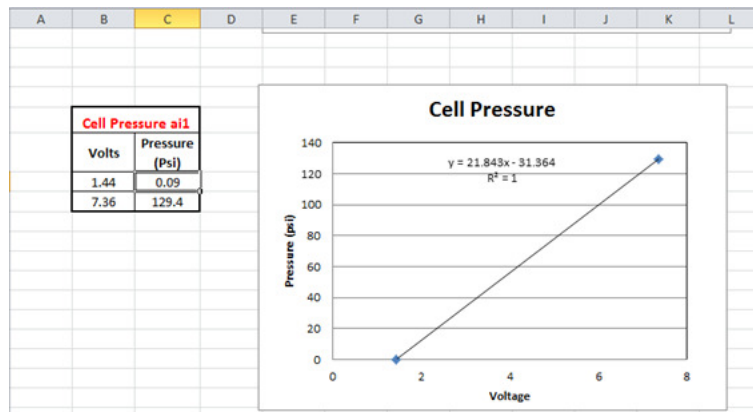


Fig. A-12—Linear regression to calculate slope and intercept for calibration line.

- Go back to the **Measurement & Automation Explorer** and double-click **NI-DAQmx Scales**.

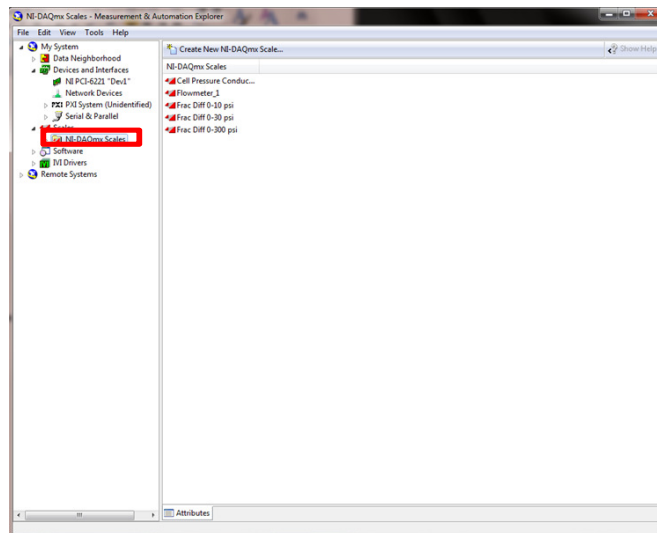


Fig. A-13—Scale selection panel.

- Select a preexistent scale located in the right panel or create a new one by clicking **Create a New NI-DAQmx Scale** button. Description of both options is presented below.
- Type the **Slope** and the **Y-Intercept** in the corresponding boxes if a preexisting scale is selected.
- Select in **Pre-Scaled** units “Volts” and “PSI” for **Scaled**. Click **Save**.

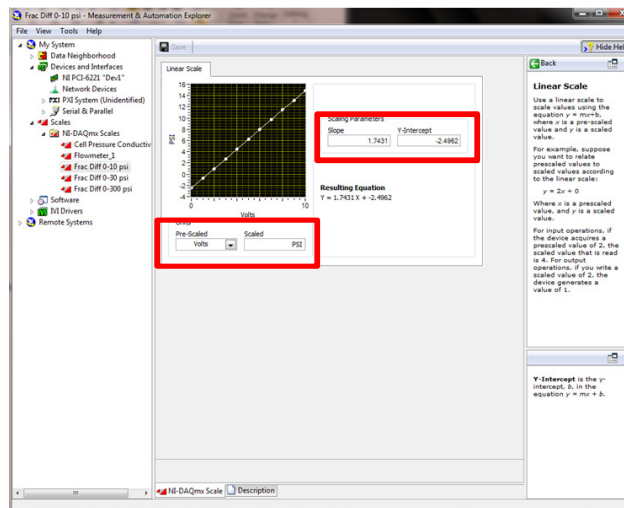


Fig. A-14—Calibration data for preexisting scale.

- Select **Linear** as the type of scale if creating a new scale.

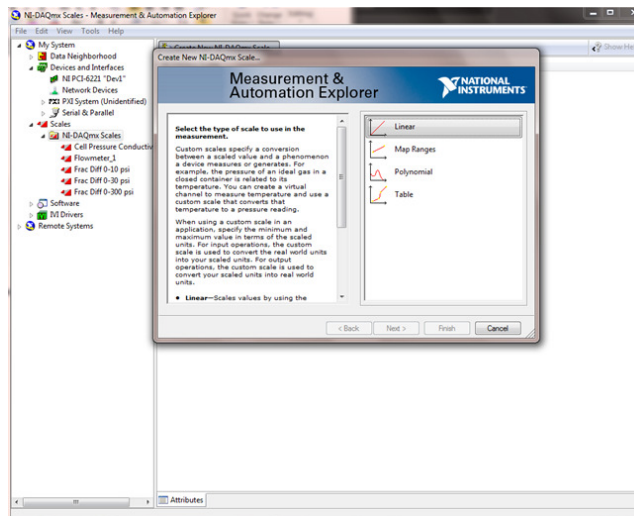


Fig. A-15—Wizard for creation of new calibration scale.

- Click **Next** and enter a name for the new scale. For this example, the default name “MyScale” is used.
- Click **Finish** and then enter the values of the **Slope** and **Y-Intercept**. As for a preexisting scale, **Pre-Scaled** units “Volts” and “PSI” for **Scaled**.

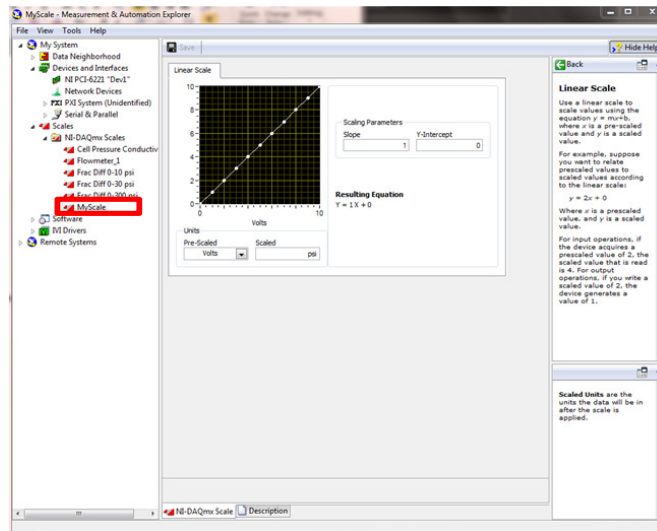
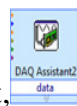
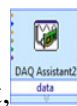



Fig. A-16—Calibration data for new scale.

- Click **Save**.
- Exit the **Measurement & Automation Explorer**.
- Open the **Acid Fra Injection ERV.vi** program.
- Go to **Window** and then **Show Block Diagram**.



- Double-click in **DAQ Assistant 2** object, , on the block diagram.
- Click **Details** button, , to see the channels settings. Select **Voltage_1** which is the corresponding to the device dev1/ai0.

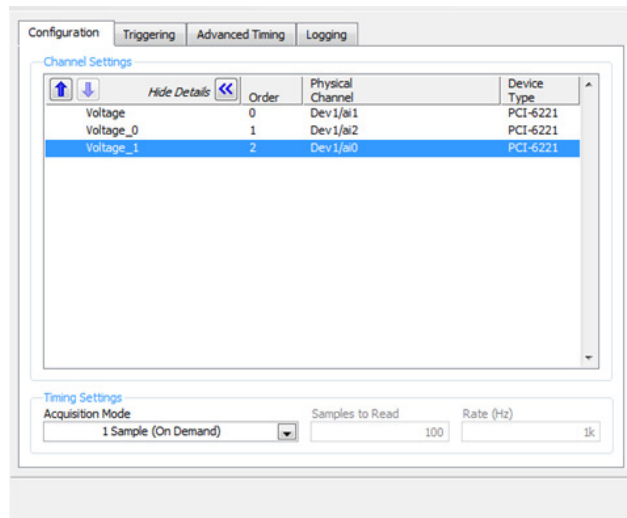
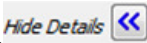


Fig. A-17—Voltage selection.

- Click **Hide Details** button, , and select MyScale in the drop-down menu **Scales**.

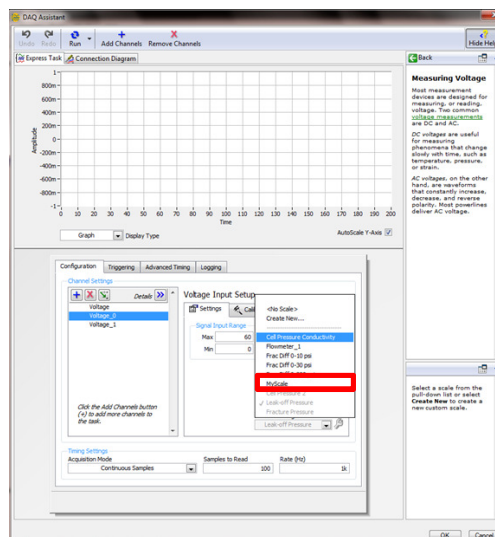


Fig. A-18—Scale selection.

- Enter the Maximum (**Max**) and Minimum (**Min**) range in **Signal Input Range** boxes. Usually, the Min range is 0 psi and Max is the upper value in the calibration line.
- Click **OK**.

APPENDIX B

B.1. Derivation of Equation for Acid Fracture Conductivity Calculations.

The starting Darcy's equation for flow in the fracture after acid injection is:

$$k_f = \frac{q_w \mu_w l_f}{A_f \Delta P} \dots\dots\dots (B-1)$$

Where k_f is the permeability in the etched fracture in m^2 , q_w is the water flow rate in m^3/s , μ_w is the water viscosity in Pa.s, l_f is the fracture length in m, A is the area of the fracture in m^2 , and ΔP is the pressure drop across the etched fracture in Pa. Converting the variables in Eq. B-1 from SI units to field units, the resulting equation is:

$$k_f = 96356.8 \frac{q_w \mu_w l_f}{A \Delta P} \dots\dots\dots (B-2)$$

Where k_f is in md, q_w is in L/min, μ_w is in cP, l_f is in in., A is in in^2 , and ΔP is in psi. Considering A_f as the product of the fracture width (w_f) and fracture height (h_f), acid fracture conductivity is defined as the product of k_f and w_f . In addition, replacing the values of h_f equivalent to 1.61 in. and l equivalent to 5.375 in., the resulting equation is:

$$k_f w = 26807.3 \frac{q_w \mu_w}{\Delta P} \dots\dots\dots (B-3)$$

Where $k_f w$ is acid fracture conductivity in md-ft. Eq.B3 is the same as aforementioned Eq. 5. The value of h_f accounts for an average value of 0.045 in. of silicon invasion in each side of the fracture surface. The value of l_f is equivalent to the distance between the two pressure ports in the conductivity cell main body.

B.2.Calculation of Matrix Conductivity

Measurements of permeability in the core samples were done using the conductivity cell. As shown in **Fig. B-1**, these measurements were down by closing the cell outlet and quantifying the flow of water through the lower core. The pressure drop across the core was measured as well.

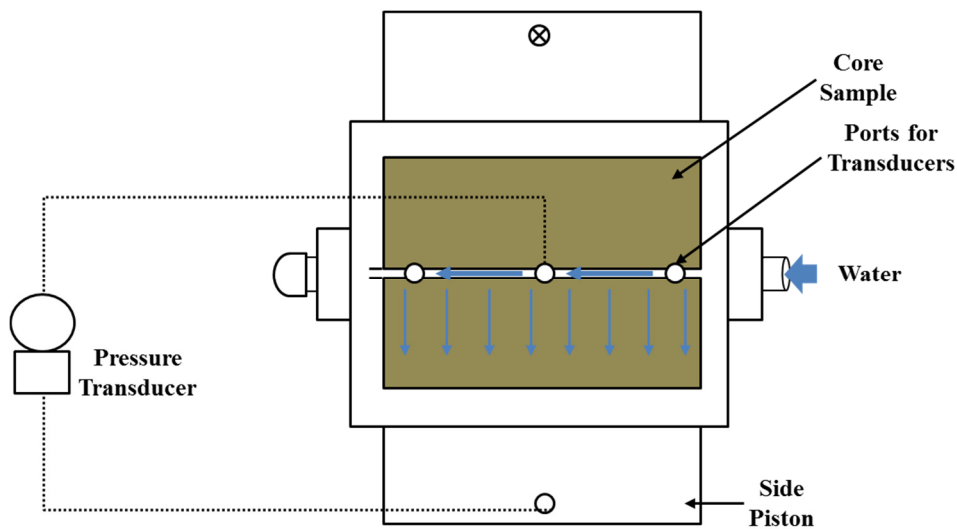


Fig. B-1—Schematic for permeability measurements using conductivity cell.

In Eq. B-2, A_f is substituted by 12.47 in² which in this case is the area of flow. Similarly, l_f is substituted as 3 in. which is the length of flow through the core. The resulting equation for matrix permeability calculations is:

$$k_m = 23181.3 \frac{q_w \mu_w}{\Delta P} \dots \dots \dots (B-4)$$

Permeability is determined when the pressure drop across the core, ΔP , reaches a stable value at a constant flow rate q_w . This value of pressure drop is then used in Eq. B-3 to calculate matrix conductivity $(k_{fw})_m$. Permeability was not measured for all the cores used in this experimental work. Random cores were selected and permeability was measured. An average permeability for these cores was 3.77 md. With this value and q_w , which was kept constant for all permeability measurements, an average pressure drop across the core, ΔP_{avg} , was calculated using Eq. B-4. Then ΔP_{avg} and q_w values are replaced in Eq. B-3 to calculate matrix conductivity which yielded 4.36 md-ft. The values of the variables mentioned above are presented in the Table B-1:

Variable	Values
Flow rate, q_w	0.002 L/min
Water viscosity at 70°F, μ_w	0.96 cp
Average pressure drop, ΔP_{avg}	11.8 psi
Matrix Conductivity, $(k_{fw})_m$	4.36 md-ft

Table B-1—Values of variables used in matrix conductivity calculation.

APPENDIX C

C.1 Top Etched Profiles of Experiments Conducted at 100 and 130 °F.

The following figures show the top etched profiles and the volume of rock dissolved by the acid of the experiments conducted at 100 and 130 °F:

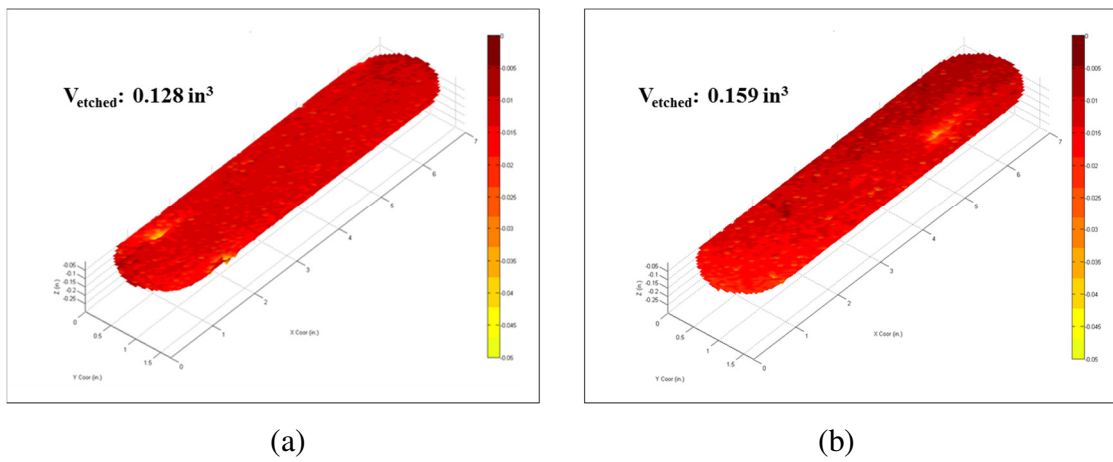


Fig. C-1—Top etched fracture surfaces and V_{etched} values of smooth surface cores. (a) 5 minutes of rock-acid contact at 100 °F, (b) 10 minutes of rock-acid contact at 100 °F.

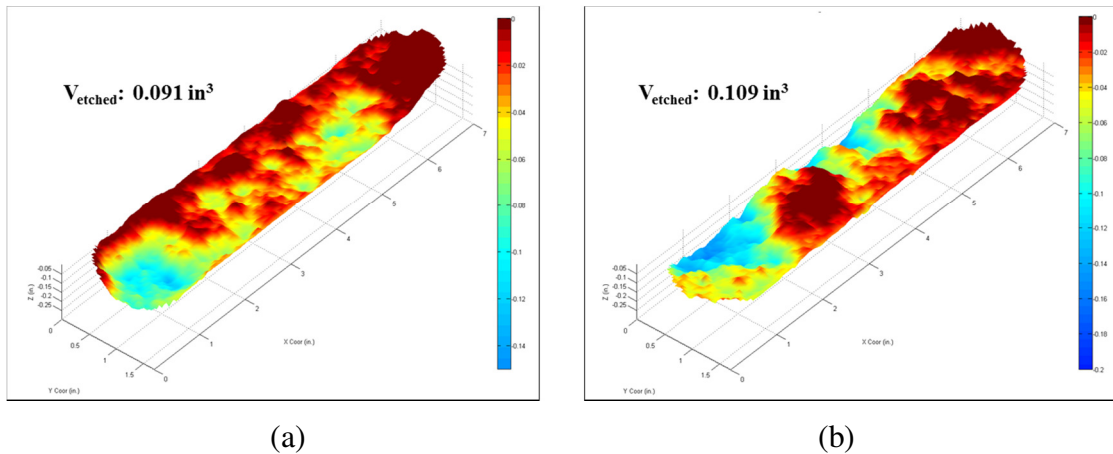


Fig. C-2—Top etched fracture surfaces and V_{etched} values of rough surface cores. (a) After 5 minutes of rock-acid contact at 100 °F, (b). After 10 minutes of rock-acid contact at 100 °F.

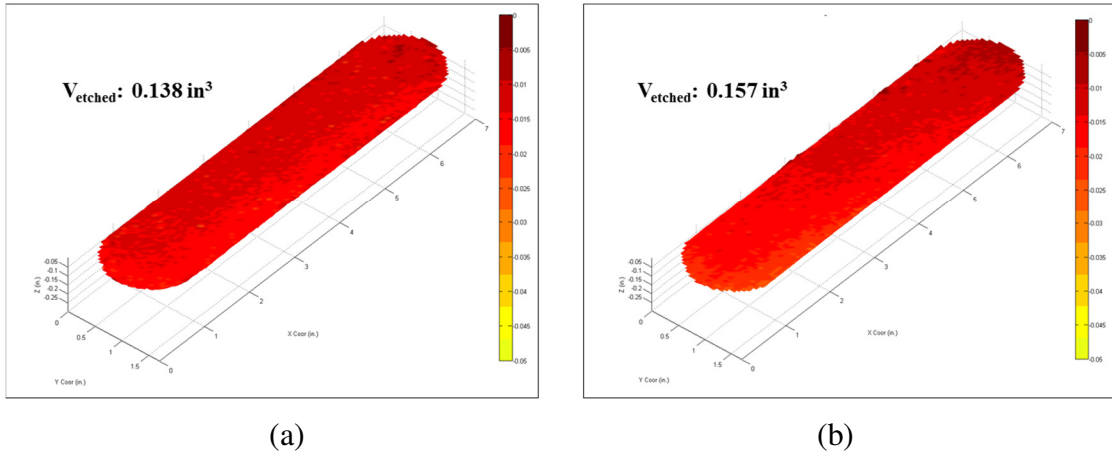


Fig. C-3—Top etched fracture surfaces and V_{etched} values of smooth surface cores. (a) 5 minutes of rock-acid contact at 130 °F, (b) 10 minutes of rock-acid contact at 130 °F.

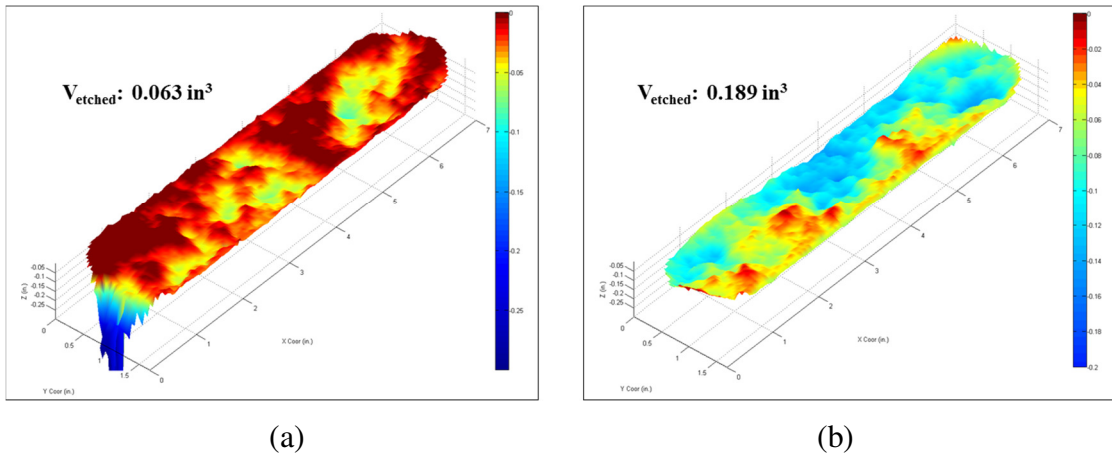


Fig. C-4—Top etched fracture surfaces and V_{etched} values of rough surface cores. (a) After 5 minutes of rock-acid contact at 130 °F, (b). After 10 minutes of rock-acid contact at 130 °F.